

Morphology of 32 Repeating Fast Radio Burst Sources at Microsecond Time Scales with CHIME/FRB

ALICE P. CURTIN,^{1,2} KETAN R. SAND,^{1,2} ZIGGY PLEUNIS,^{3,4} NAMAN JAIN,⁵ VICTORIA KASPI,^{1,2} DANIELE MICHILLI,^{6,7} EMMANUEL FONSECA,^{8,9} KAITLYN SHIN,^{6,7} KENZIE NIMMO,⁶ CHARANJOT BRAR,¹⁰ FENGQIU ADAM DONG,^{11,12} GWENDOLYN M. EADIE,^{13,14} B. M. GAENSLER,^{15,16,13} ANTONIO HERRERA-MARTIN,^{13,17} ADAEZE L. IBIK,^{16,13} RONNIY C. JOSEPH,^{1,2} JANE KACZMAREK,¹⁸ CALVIN LEUNG,^{19,20} ROBERT MAIN,¹ KIYOSHI W. MASUI,^{6,7} RYAN MCKINVEN,^{1,2} JUAN MENA-PARRA,^{16,13} CHERRY NG,²¹ AYUSH PANDHI,^{13,16} AARON B. PEARLMAN,^{1,2} MASOUD RAFIEI-RAVANDI,¹ MAWSON W. SAMMONS,^{1,2} PAUL SCHOLZ,^{22,16} KENDRICK SMITH,²³ AND INGRID STAIRS¹¹

¹Department of Physics, McGill University, 3600 rue University, Montréal, QC H3A 2T8, Canada

²Trottier Space Institute, McGill University, 3550 rue University, Montréal, QC H3A 2A7, Canada

³Anton Pannekoek Institute for Astronomy, University of Amsterdam, Science Park 904, 1098 XH Amsterdam, The Netherlands

⁴ASTRON, Netherlands Institute for Radio Astronomy, Oude Hoogeveensedijk 4, 7991 PD Dwingeloo, The Netherlands

⁵McGill

⁶MIT Kavli Institute for Astrophysics and Space Research, Massachusetts Institute of Technology, 77 Massachusetts Ave, Cambridge, MA 02139, USA

⁷Department of Physics, Massachusetts Institute of Technology, 77 Massachusetts Ave, Cambridge, MA 02139, USA

⁸Department of Physics and Astronomy, West Virginia University, PO Box 6315, Morgantown, WV 26506, USA

⁹Center for Gravitational Waves and Cosmology, West Virginia University, Chestnut Ridge Research Building, Morgantown, WV 26505, USA

¹⁰National Research Council of Canada, Herzberg Astronomy and Astrophysics, 5071 West Saanich Road, Victoria, BC V9E2E7, Canada

¹¹Department of Physics and Astronomy, University of British Columbia, 6224 Agricultural Road, Vancouver, BC V6T 1Z1 Canada

¹²National Radio Astronomy Observatory, 520 Edgemont Rd, Charlottesville, VA 22903, USA

¹³David A. Dunlap Department of Astronomy and Astrophysics, 50 St. George Street, University of Toronto, ON M5S 3H4, Canada

¹⁴Department of Statistical Sciences

¹⁵Department of Astronomy and Astrophysics, University of California Santa Cruz, 1156 High Street, Santa Cruz, CA 95060, USA

¹⁶Dunlap Institute for Astronomy and Astrophysics, 50 St. George Street, University of Toronto, ON M5S 3H4, Canada

¹⁷Department of Statistical Science, University of Toronto, Ontario Power Building, 700 University Avenue, 9th Floor, Toronto, ON M5G 1Z5, Toronto, Ontario, Canada

¹⁸CSIRO Space & Astronomy, Parkes Observatory, P.O. Box 276, Parkes NSW 2870, Australia

¹⁹Department of Astronomy, University of California, Berkeley, CA 94720, United States

²⁰NASA Hubble Fellowship Program (NHFP) Einstein Fellow

²¹Laboratoire de Physique et Chimie de l'Environnement et de l'Espace (LPC2E) UMR7328, Université d'Orléans, CNRS, F-45071 Orléans, France

²²Department of Physics and Astronomy, York University, 4700 Keele Street, Toronto, ON M3J 1P3, Canada

²³Perimeter Institute of Theoretical Physics, 31 Caroline Street North, Waterloo, ON N2L 2Y5, Canada

Submitted to ApJ

ABSTRACT

The Canadian Hydrogen Intensity Mapping Experiment Fast Radio Burst (CHIME/FRB) project has discovered the most repeating fast radio burst (FRB) sources of any telescope. However, most of the physical conclusions derived from this sample are based on data with a time resolution of ~ 1 ms. In this work, we present for the first time a morphological analysis of the raw voltage data for 118 bursts from 32 of CHIME/FRB's repeating sources. We do not find any significant correlations amongst fluence, dispersion measure (DM), burst rate, and burst duration. Performing the first large-scale morphological comparison at timescales down to microseconds between our repeating sources and 125 non-repeating FRBs, we find that repeaters are narrower in frequency and broader in duration than

non-repeaters, supporting previous findings. However, we find that the duration-normalized sub-burst widths of the two populations are consistent, possibly suggesting a shared physical emission mechanism. Additionally, we find that the spectral fluences of the two are consistent. When combined with the larger bandwidths and previously found larger DMs of non-repeaters, this suggests that non-repeaters may have higher intrinsic specific energies than repeating FRBs. We do not find any consistent increase or decrease in the DM ($\lesssim 1 \text{ pc cm}^{-3} \text{ yr}^{-1}$) and scattering timescales ($\lesssim 2 \text{ ms yr}^{-1}$) of our sources over $\sim 2 - 4$ year periods.

Keywords: Fast Radio Bursts, Radio transient sources

1. INTRODUCTION

Fast radio bursts (FRBs) are brief ($\mu\text{s} - \text{ms}$) bursts of radio emission originating from primarily extragalactic distances with radio luminosities $\sim 10^{36} - 10^{44} \text{ erg s}^{-1}$ (Lorimer et al. 2007). FRBs are typically divided into non-repeating (or “one-off”) FRBs (CHIME/FRB Collaboration et al. 2021) and repeating FRBs (Spitler et al. 2016; CHIME/FRB Collaboration et al. 2019a,b, 2023a; Fonseca et al. 2020). While most FRBs’ repeatability is seemingly uncorrelated, one source shows definitive periodic windows of burst activity (CHIME/FRB Collaboration et al. 2020a).

Despite the large number of published FRBs, the progenitors and emission mechanisms of these sources remain uncertain. The detection of an FRB-like burst from the Galactic magnetar SGR 1935+2154 lent strong evidence to magnetars as possible progenitors (CHIME/FRB Collaboration et al. 2020b; Bochenek et al. 2020). However, the discovery of a repeating FRB in the globular cluster of M81 challenged this hypothesis, as magnetars are unexpected in such old environments (Bhardwaj et al. 2021; Kirsten et al. 2022).

Theoretical models for the emission mechanism generally involve neutron stars (NS), and fall into two main categories: those that suggest emission arises from a synchrotron maser process driven by shocks far from the central compact object (Metzger et al. 2019), and those that propose the emission originates closer to the central compact object, such as within the magnetosphere (Lu & Kumar 2018; Ioka 2020). Recent evidence has increasingly supported the idea of a magnetospheric origin for at least some sources (CHIME/FRB Collaboration et al. 2020a; Nimmo et al. 2021; Nimmo et al. 2022; Mckinven et al. 2024; Nimmo et al. 2024).

It also remains uncertain whether repeating and non-repeating FRBs represent two distinct classes of objects. Modeling of the FRB population has shown that the Canadian Hydrogen Intensity Mapping Experiment Fast Radio Burst (CHIME/FRB) sample is consistent with all FRBs being repeaters (James 2023). However, there are distinct differences between the morphologi-

cal properties of these two classes. A large-scale study of the morphological features of repeating versus non-repeating FRBs using CHIME/FRB was first presented by Pleunis et al. (2021a). They confirmed that repeating FRBs often exhibit a pattern referred to as the “sadtrombone effect” wherein the emission marches downward in frequency with time (and herein referred to as downward drifting; Gajjar et al. 2018; Hessels et al. 2019). Additionally, the temporal duration of repeating FRBs tends to be larger while the bandwidth is narrower than that of non-repeaters.

The results of Pleunis et al. (2021a) were based on intensity data from CHIME/FRB with a time resolution of 0.983 s. However, there is evidence that FRBs have complex morphology that can only be seen at high-time resolution (e.g., Faber et al. 2023). High-time resolution observations ($\sim \mu\text{s}$) have demonstrated the potential to:

- **Improve Dispersion Measure Estimations:** Given the extragalactic distances of FRBs, the emitted radio waves will be dispersed by ionized electrons along the line-of-sight (LOS), resulting in a frequency-dependent dispersion sweep of the radio emission at the location of the telescope. This dispersion sweep can be used to calculate a dispersion measure (DM) per source and is directly proportional to the LOS integrated electron density between the source and the observer. This DM consists of components from the Milky Way, intergalactic medium (IGM), host galaxy, and local environment. The contributions from the Milky Way, IGM, and host galaxy are not expected to vary significantly with time, such that temporal variations in the DM of a source can typically be attributed to the local host environment. Microsecond features within a burst enable precise alignment of burst characteristics, facilitating accurate per-burst DM determinations. This allows us to disentangle the true DM from frequency-dependent features such as downward drifting of the burst in frequency with time. Such measurements are crucial for investigating DM variations

over time in repeating FRBs, providing valuable insights into the FRB’s local environment (e.g., Yang & Zhang 2016; Hessels et al. 2019; Piro & Gaensler 2018; Sand et al. 2023).

- **Investigate potential intra-burst DM variations:** Observations at high time resolution may reveal DM variations between different components of a single burst, as possibly identified by Faber et al. (2023), Hewitt et al. (2023), and Sand et al. (2024). Intra-burst DM variations might suggest a highly dense, local environment such as a supernovae remnant, bow shock and/or different emitting heights for the various sub-components.
- **Search for Periodicity:** By distinguishing various components within a burst, we can search for quasi-periodic or periodic structures, as shown by CHIME/FRB Collaboration et al. (2022). Kramer et al. (2024) found that all radio-loud magnetars show signs of quasi-periodic structure. They suggested that this structure in the emission was directly related to the magnetar’s rotational spin period. Thus, \sim millisecond-duration periodic features in FRB emission would strongly lend support for a magnetospheric emission mechanism for FRBs.
- **Identify and distinguish downward drifting:** Downward drifting can often be indistinguishable from small dispersion delays and/or scattering at \sim ms time resolution (Sand et al. 2024). This feature could arise either from emission in a NS magnetosphere (Wang et al. 2019) or through the deceleration of shock waves farther from the source (Margalit et al. 2020).
- **Measure Scattering Timescales:** Measuring accurate scattering timescales for sources gives insight into their local and host environments along with that of intervening plasma in galaxy halos and the intergalactic medium (Chawla et al. 2022).
- **Detect μ s or ns-scale features:** Some FRBs exhibit extremely short timescale features known as micro features and nano-shots (Farah et al. 2018; Cho et al. 2020; Nimmo et al. 2021; Majid et al. 2021; Nimmo et al. 2022; Hewitt et al. 2023). Such features again strongly support magnetospheric emission models for at least for the sources that exhibit them (Nimmo et al. 2021). There has not, however, been a large-scale analysis of the microstructure of repeating versus non-repeating sources.

CHIME/FRB Collaboration et al. (2024) recently published the complex raw voltages for 140 of the FRBs from the first CHIME/FRB catalog (CHIME/FRB Col-

laboration et al. 2021). This dataset enabled accurate flux and fluence measurements for these bursts, a critical improvement as CHIME/FRB intensity fluxes/fluences are only lower limits (CHIME/FRB Collaboration et al. 2021). Sand et al. (2024) analyzed the morphology of these bursts at timescales down to 2.56 μ s. They found that non-repeating FRBs also show complex morphology similar to repeaters. Their sample consisted of 125 bursts from thus-far non-repeaters and 12 bursts from repeaters, the largest sample of individual FRB sources studied at such high time resolutions. However, no work has studied a similarly large number of repeating sources at such high-time resolution.

In this paper, we present the first large-scale study of the morphology of repeating FRBs at time resolutions down to 2.56 μ s using the CHIME/FRB experiment. In Section 2, we discuss the CHIME/FRB instrument, its complex voltage recording system, and the analysis pipeline used to determine burst properties. In Section 3, we present the sources analyzed in this work. In Section 4, we present various analyses related to the burst properties. We start by searching for correlations amongst various morphological parameters for our repeating FRB dataset. We then compare the morphological parameters of the repeating FRBs with those of the non-repeating FRBs studied by Sand et al. (2024). Finally, we explore whether any of our repeaters show changing environments with time. In Section 5, we discuss our results in the context of the FRB population. We end in Section 6 by summarizing our work.

2. CHIME/FRB INSTRUMENT & ANALYSIS PIPELINES

2.1. Instrument

The CHIME telescope is located near Penticton, British Columbia and consists of four fixed cylindrical parabolic reflectors oriented in the N-S direction. Each cylinder has 256 dual polarization feeds operating from 400 to 800 MHz. CHIME’s total field-of-view (FOV) is \sim 250 deg², with a N-S FOV of \sim 120° and a frequency-dependent E-W FOV of \sim 1.3–2.5° (see Ng et al. 2017, for more details). The output of CHIME’s 1024 antenna signals are first sent to an FX-correlator which digitizes the output and then forms 1024 intensity beams with a time resolution of 0.983 ms and frequency resolution of 24.4 kHz on the sky (Chikada et al. 1984; Ng et al. 2017; CHIME Collaboration et al. 2022; Andersen et al. 2023). These formed beams are searched for FRB signals by first performing a radio frequency interference (RFI) removal algorithm (Rafiei-Ravandi & Smith 2022) and then iteratively searching over DM-space for possible astrophysical signals. FRB candidates are passed

to a machine learning algorithm that further removes RFI. The final set of FRBs (e.g., those published by [CHIME/FRB Collaboration et al. 2021](#)) are verified by CHIME members. Further details on this pipeline can be found in [CHIME/FRB Collaboration et al. \(2018\)](#).

CHIME/FRB is equipped with a complex voltage recording system (referred to as the ‘baseband system’) that constantly buffers ~ 20 seconds of channelized (1024 channels over 400 MHz) data with a time resolution of $2.56 \mu\text{s}$ ([Michilli et al. 2021](#)). When an FRB with a $S/N \gtrsim 12$ is identified by the real-time system, the system triggers ~ 100 ms of data to be saved around the de-dispersed pulse for offline analysis.

Capturing the complex voltages offers significant advantages in addition to that of providing a high-time resolution dataset. One key benefit is the ability to directly beamform¹ the data which greatly improves the initial localization of the source and avoids the spectral artifacts of the FFT. For CHIME/FRB, initial real-time localizations can span several degrees in RA and approximately 0.5 degrees in Dec. However, with this system, localizations on the order of arcminutes (and sometimes even ~ 10 arcsec) are achievable depending on the S/N of the burst ([Michilli et al. 2023](#); [CHIME/FRB Collaboration et al. 2023b](#)). Additionally, by correcting for the beam response of CHIME/FRB, these data enable significantly more accurate determinations of fluxes and fluences for bursts ([CHIME/FRB Collaboration et al. 2023b](#); [Sand et al. 2024](#)).

2.2. Analysis Pipeline

The pipeline deployed in this work to analyze the complex raw voltages and determine the burst parameters has been described in detail by [Sand et al. \(2023, 2024\)](#). The output of this pipeline is: a structure-maximized DM, a flux/fluence for each burst, the number of distinct sub-bursts for an FRB at the given time resolution, the width of each sub-burst, the full duration and bandwidth of the burst, a DM determined using a 2D spectro-temporal fit, and a scattering time measured using the same 2D spectro-temporal fit (if applicable). Below, we provide a brief overview of each step of this pipeline from initial collection of the complex raw voltages to the final burst fits.

Step 1: The complex raw voltages are first beamformed to the previously published best-position for each repeater ([Michilli et al. 2023](#); [CHIME/FRB Collaboration et al. 2023a](#)) and coherently de-dispersed to the

best known DM of the source. RFI masking is also performed.

Step 2: The data are downsampled from a time resolution of $2.56 \mu\text{s}$ such that a minimum peak S/N of $\sim 10 - 15$ is reached for each burst. The S/N limit is chosen on a burst-to-burst basis given burst characteristics. If a burst has not reached the desired S/N threshold at a time resolution of 0.655 ms, we either a) remove the burst from our sample or b) include the burst but caution that the parameter fit (discussed below) may be less reliable.

Step 3: We determine a DM by maximizing S/N for the burst. We use this DM as an input to search for a structure-optimized DM using the `DM phase` routine ([Seymour et al. 2019](#)).

Step 4: We determine a profile for the burst by summing over all non-RFI channels. We then smooth the profile using a locally weighted scatter plot smoothing method (LOWESS) implemented by `statsmodel` in python ([Seabold & Perktold 2010](#)). We then determine the number of peaks within the burst using the `find_peaks` algorithm implemented by `SciPy` ([Virtanen et al. 2020](#)). In certain cases, we manually supply the number of peaks when the `find_peaks` algorithm does not pick out the same number of peaks as determined by eye.

Step 5a: To determine the initial temporal profile parameters, we fit a sum of exponentially modified Gaussians (EMGs; [McKinnon 2014](#)), with one Gaussian per sub-burst using the nonlinear least-squares algorithm `curve_fit` from `SciPy`. The same scattering timescale is assumed for each sub-burst.

Step 5b: In certain cases, a visual inspection of the results of the least-squares algorithm for the initial profile parameters does not provide a sufficient fit to the data. In these cases, we use the `emcee` routine to employ a Markov Chain Monte Carlo (MCMC) algorithm to fit for the profile parameters ([Foreman-Mackey et al. 2013](#)).

Step 6: We provide these initial temporal profile parameters to `fitburst`, a 2D spectro-temporal fitting routine that uses a combination of EMGs to model the data ([Fonseca et al. 2023](#)). The data are first fit assuming no scattering contribution. The output of this no-scattering fit is then re-fed into `fitburst` to fit for scattering using EMGs. The output of `fitburst` is a 1σ width per sub-burst, a spectral index and spectral running per sub-burst, the arrival time of each sub-burst, the best-fit DM for all sub-bursts, and the best fit scattering timescale for all sub-bursts (if applicable).

Step 7: There is significant degeneracy between scattering and downward drifting. Thus, for each burst,

¹ Beamforming refers to the process in which the raw voltages are phase-referenced to a given location.

we visually decide between a no-scattering and scattering fit for the final parameters. In the majority of cases ($\sim 80\%$), the no-scattering fit is chosen. Upper limits on the scattering are reported as the reported `fitburst` width of the narrowest sub-burst component for that given burst. Simulations by Sand et al. (2024) showed that this was a reasonable limit on the scattering timescale. The reference frequency for these scattering measurements is 600 MHz, the centre of the CHIME/FRB band.

Step 8: We use the `fitburst` parameters to determine the duration of the burst. For a single component burst, we define the burst duration as the full-width half-maximum (FWHM) of that single component. For a multi-component burst, we define the burst duration as: $w_{\text{tot}} = (\text{TOA}_f + 1.2w_f) - (\text{TOA}_i + 1.2w_i)$ where f indicates the TOA for the final sub-burst and i is the TOA for the first sub-burst. The factor of ~ 1.2 translates the reported 1σ Gaussian width to half of the FWHM of that sub-burst.

Step 9: We also use the `fitburst` parameters to determine the bandwidth of the burst. Assuming a running-power law model, we use the spectral indices and spectral-running to reconstruct the spectral model per sub-burst. Then, we determine the highest and lowest frequency per sub-burst using the full-width tenth-max of the running power-law. The bandwidth is then taken to be the difference between the highest frequency channel and the lowest frequency channel from all the sub-bursts.

Step 10: We determine a flux and fluence for each burst using the method discussed by CHIME/FRB Collaboration et al. (2024).

Certain FRBs in our sample show downward drifting or complex spectral structure that is not well fit using `fitburst`. For example, some downward drifting bursts show multiple distinct components that can easily be identified and fit (e.g., see FRB 20190611A and FRB 20201228A in Figure A1) while bursts with a single downward drifting component cannot be well fit using Gaussian components (as `fitburst` tries to do, e.g., see FRB 20211104B in Figure A1). Thus, the amplitude of the components fit using `fitburst` are not consistently reliable throughout our sample (and hence are not directly used in the analysis that follows). We visually confirm that all fits at least properly encompass the number of components, arrival times, DM, sub-component widths, and sub-component bandwidths.

2.3. Burst Rates

For all sources in our sample with two or more bursts for which the complex raw voltages were captured, we

update the burst rates. Circumpolar sources ($\delta > 70^\circ$) are detected both in an upper and lower transit overhead CHIME. Similar to CHIME/FRB Collaboration et al. (2023a), we only calculate rates for the upper transit of each source.

We follow the methodology outlined by CHIME/FRB Collaboration et al. (2023a) to determine burst rates. In brief, we calculate the total exposure time for each source based on its improved position (CHIME/FRB Collaboration et al. 2023a; Michilli et al. 2023), and determine the number of bursts found within the FWHM of their detection beam at 600 MHz. We assume a Poissonian uncertainty on the burst rate, as this dominates over the uncertainty in exposure due to the improved source positions from the beam-formed data.

We calculate a spectral fluence threshold per source using the method outlined by Josephy et al. (2019). The fluence threshold accounts for three factors - day-to-day instrument gain variations, changes in synthesized beam response during source transit, and varying emission bandwidths and frequency centers. We simulate thresholds for different detection scenarios to estimate relative sensitivity between simulated and real detections, scaling the initial fluence threshold inferred from the real detection by the simulated thresholds. For repeaters, each realization of the simulation uses a randomly selected burst as the reference for determining relative sensitivity and initial threshold. Using the 95th percentile of the scaled threshold distribution per source, we scale each source's burst rate to a fluence threshold of 5 Jy ms assuming a power-law index of -1.5 for the cumulative energy distribution.

2.4. Biases

The CHIME/FRB system for recording the complex raw voltages has a number of biases in addition to those discussed for the real-time system by Merryfield et al. (2023). The full data can only be saved for sources with a $\text{DM} < 1000 \text{ pc cm}^{-3}$ due to the size of the buffer for this system, with channels at the top of the band lost. Three sources in our sample, FRB 20200809E, FRB 20190417A, and FRB 20190216A, have a $\text{DM} > 1000 \text{ pc cm}^{-3}$. Second, only ~ 100 ms of data are saved around a given event (after de-dispersion). Thus, events significantly longer than 100 ms, or events for which the initial DM was inaccurately determined, can be clipped. Certain events also lack data at all frequency channels due to issues with the early recording system. Additionally, only events above a given S/N threshold will trigger this recording system. This threshold is different for known-repeating ($\text{S/N} \gtrsim 10$) and non-repeating FRBs ($\text{S/N} \gtrsim 12$). In both cases, faint bursts or bursts

with particularly complex structure for which the peak S/N is low may be missed. While some of the selection biases of CHIME/FRB have been described by [Merryfield et al. \(2023\)](#), the selection biases against complex, narrow-band bursts (such as those studied here) has not been well studied. Lastly, [Sand et al. \(2024\)](#) found that bursts studied at time resolutions < 1 ms tended to have higher peak flux densities. This suggested that CHIME/FRB may be missing ultra-narrow bursts that do not have such high peak flux densities due to the averaging of these bursts with noise at time resolutions of 0.983 ms.

3. REPEATING FRB SOURCES

The CHIME/FRB collaboration previously published 45 repeating sources of FRBs ([CHIME/FRB Collaboration et al. 2019a,b, 2023a](#); [Fonseca et al. 2020](#); [Bhardwaj et al. 2021](#); [Lanman et al. 2022](#)). Here, we focus on the sources published in the above works that have at least one CHIME-detected burst with the complex raw voltages recorded. We do not include FRB 20180916B in our work as there has already been significant analysis of this FRB at high-time resolution with CHIME/FRB ([Sand et al. 2023](#)). We exclude two highly active, previously published repeaters detected by CHIME/FRB: FRB 20201124A and FRB 20220912A. We also do not include bursts for which the S/N at a time resolution of 0.655 ms is < 5 . The remainder amounts to 118 bursts with recorded complex raw voltages from 32 repeating FRBs between 2018 August and 2023 September. The end date is chosen to be consistent with the cutoff for the second CHIME/FRB catalog that is in preparation.

We present a sub-sample of the frequency versus time (hereafter referred to as ‘waterfall’) plots in the Appendix in [Figure A1](#). We also list each burst and its fit parameters in [Table A1](#). We could not determine a flux/fluence measurement for four repeater bursts in our sample (FRB 20190626A, FRB 20191217A, FRB 20210302E and FRB 20220203A) as they were detected $> 2^\circ$ from the meridian of CHIME/FRB where our primary beam model is not sufficiently well understood. We also could not determine a flux/fluence for FRB 20210130E due to its low S/N. In [Table A2](#), we present the updated burst rates for our sources.

4. RESULTS

4.1. Burst Property Correlations

In [Figure 1](#), we plot various combinations of burst rate, average source duration, average source fluence, and extragalactic (+halo) DM in order to search for correlations. While we primarily focus on repeating FRBs for these correlations, we include non-repeaters

from [Sand et al. \(2024\)](#) in some of the comparisons for which it makes sense to do so (e.g., correlations not including burst rate). For the average burst duration and fluence, the plotted error bars encapsulate the range of values for that source, e.g., the range of burst durations exhibited by that repeater over all of its bursts.

We define the extragalactic DM as the excess after subtracting the NE2001 Galactic component ([Cordes & Lazio 2002](#)) from the DM determined using `fitburst`. We assume a 20% uncertainty on the NE2001 DM contribution. While some models and constraints on the Milky Way halo predict significant latitude-dependent structure (e.g., [Yamasaki & Totani 2020](#); [Das et al. 2021](#)), the variation between the median DM halo values from most commonly accepted models is of order that expected from the variations along individual lines-of-sight ([Cook et al. 2023](#)). Thus, we do not account for the halo contribution to the observed DMs. This has the same effect on the analysis as would subtracting a constant halo value from each line of sight. We refer to this DM as the extragalactic DM (+halo). We do not account for the Galactic scattering contribution, as it is not additive in the same way as the DM. However, all of our scattering values are significantly larger than the predicted Galactic scattering contribution ([Cordes & Lazio 2002](#)). We also only include sources in our analysis for which there are at least two bursts from that source that have the complex raw voltages recorded. This totals 25 different repeating sources.

To determine whether a given correlation is significant, we use the [Spearman \(1904\)](#) rank test as implemented in python using `scipy.stats.spearmanr` ([Virtanen et al. 2020](#)). For a correlation to be considered significant, we require the Spearman p -value to be to be $p < 10^{-3}$.

To account for uncertainties in our measured parameters, we follow the technique presented by [CHIME/FRB Collaboration et al. \(2023a\)](#). We first perform a Monte Carlo (MC) simulation in which we re-determine a given parameter (e.g., average duration of a source) 1000 times. We do this by sampling from the uncertainty region for each burst for that given parameter in order to determine a new average parameter. We calculate an associated Spearman p -value and correlation coefficient for every iteration, and report the median p -value and correlation coefficient from the MC along with the Median Absolute Deviation From the Median (MADFM).

4.1.1. Burst Rate & Average Duration

As seen in the top left panel of [Figure 1](#), we do not find a significant correlation between burst rate and average burst duration. [Connor et al. \(2020\)](#) suggested that the

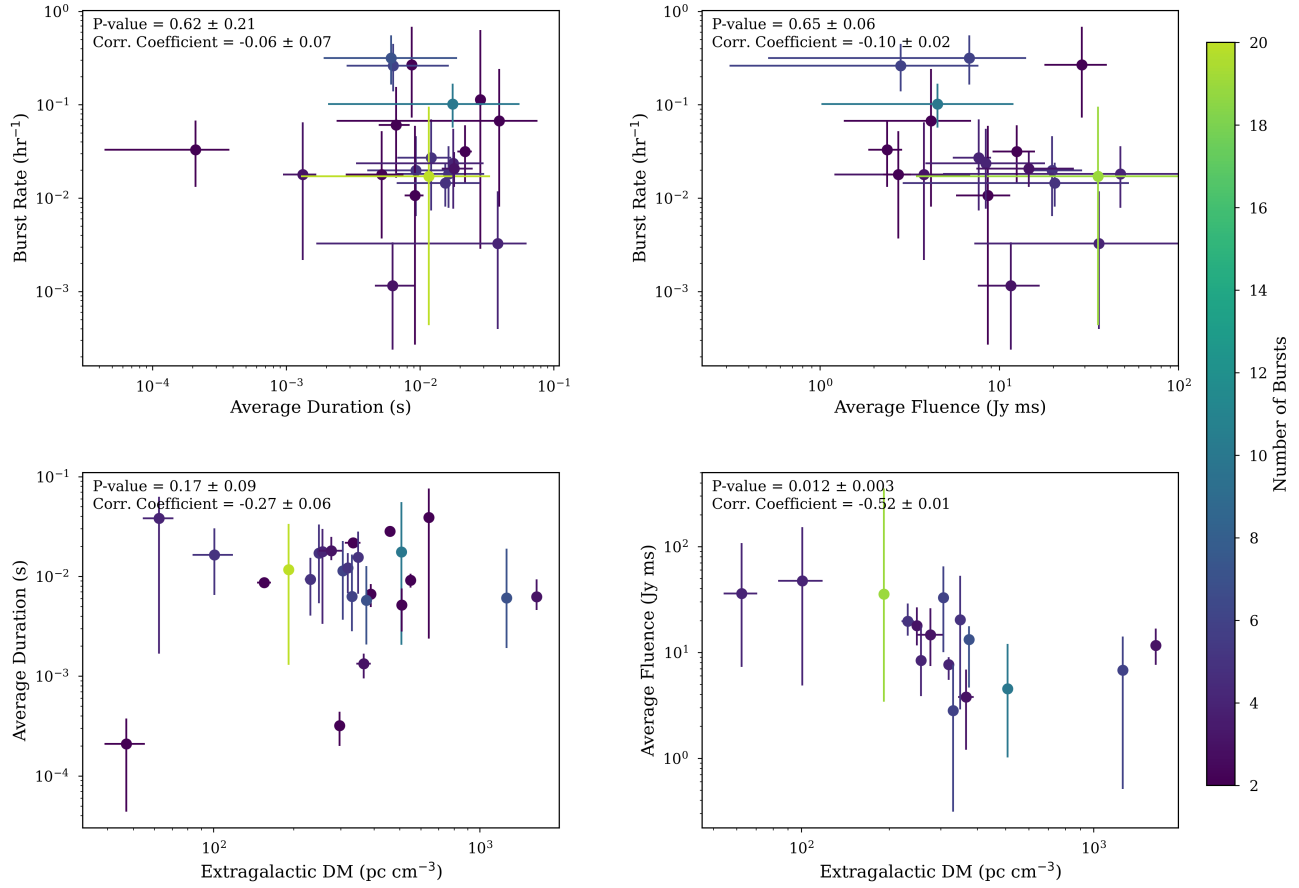


Figure 1. Correlations amongst burst rate, average burst duration, average burst fluence, and extragalactic (+halo) DM for the repeating FRBs in our sample. As discussed in Section 4.1, we do not subtract a Galactic halo contribution from the total DM. We only include sources for which we have ≥ 2 bursts with the complex raw voltages recorded. The shown Spearman p -values and correlation coefficients are the median value from 1000 MC iterations in which we iterate over the measured parameter uncertainties and calculate a new p -value and correlation coefficient at each iteration. Uncertainties are calculated using the MADFM.

burst rate and duration of FRBs may be correlated in order to explain the discrepancies in the widths of repeating and non-repeating FRBs observed in Pleunis et al. (2021a). If the beaming angle of a source is directly related to the burst width, we would expect fewer bursts from sources emitting narrow bursts, as their emission would be highly beamed.

However, as seen in Figure 1, many sources emit bursts spanning approximately an order of magnitude in burst duration, with FRB 20181030A emitting bursts over approximately two orders of magnitude in duration. If beaming angle is proportional to burst width, then this implies a significant change in the beaming angle for an individual source. It is also possible that the large range of burst durations seen from a given source obscures an underlying correlation. Therefore we also re-do the correlation study using only the maximum burst width from a given source (see Figure A2 in the Appendix). The median p -value from 1000 MC sam-

ples for this correlation is 0.096. While this is smaller than that using average burst duration, it is still not significant.

It is also possible that the large burst rate uncertainties (dominated by the number of bursts due to the assumed Poissonian nature) obscure an underlying correlation here. CHIME/FRB is also biased against detecting long bursts (Merryfield et al. 2023) and the sensitivity of the instrument to highly complex bursts (such as downward drifting bursts) is not yet quantified. Thus, it is possible that CHIME/FRB is missing the longest bursts from these sources, and hence we are not yet probing the widths needed to see a burst rate versus duration correlation. The burst rates and durations here are also determined in the observer’s reference frame, while that predicted by Connor et al. (2020) are in the burst reference frame.

Nonetheless, our results may suggest that there is significant jitter in the relation between burst duration and

beaming angle, or that burst duration is not correlated with the beaming angle for the radio emission. As discussed by Connor et al. (2020), emission models involving shocks far from a central compact object predict a direct scaling of pulse width with beaming angle. However, models involving emission close to the surface of a NS do not as clearly predict this correlation.

4.1.2. Burst rate & Average Fluence Correlation

As seen in top right panel of Figure 1, we do not find a significant correlation between burst rate and a source’s average fluence. Theoretically, such a correlation might be expected if all FRBs share the same luminosity function and average luminosity, as nearby repeaters would be more likely to have a higher observed burst rate and higher average fluence. However, this correlation is likely heavily affected by our detection threshold, with our average fluences biased high due to our inability to detect low fluence events. Additionally, this comparison may be affected by our reduced ability to detect long duration bursts with high fluences (Merryfield et al. 2023). If indeed the lack of a correlation is astrophysical and is not impacted by our system biases, it suggests that repeating FRBs have a wide range of average intrinsic luminosities.

4.1.3. Average Duration & Extragalactic DM Correlation

As seen in the bottom left panel of Figure 4.1, we do not find a significant correlation between the average duration of our sources and their extragalactic (+halo) DM, as might be expected if higher-DM sources are on average farther away and undergo greater cosmological time dilation (Connor 2019). We also re-do this analysis including the non-repeating bursts from Sand et al. (2024) as this analysis does not require a burst repetition rate. The p -value for the correlation using this additional sample of bursts is 0.98, which is not significant (see Figure A3 in the Appendix).

Using the first CHIME/FRB catalog, Shin et al. (2023) predicted that 99.4% of CHIME/FRB sources would be found at redshifts ≤ 2 . A redshift of 2 corresponds to a cosmological expansion factor of 3. Given that the burst duration from a given source can vary by an order of magnitude, the effect of a cosmological expansion factor is likely too small at these redshifts to be discernible. Additionally, propagation effects such as multiple scattering screens may smear out such effects (Sand et al. 2024).

4.1.4. Average Fluence & Extragalactic DM Correlation

As seen in the lower left panel of Figure 1, we do not find a correlation between the average fluence of our sources and their extragalactic (+halo) DM, as might

be expected if higher-DM sources are on average farther away and all repeating FRBs follow a universal luminosity function with the same average luminosity. We re-do the correlation using the median fluence, but again find no correlation. We also re-do the correlation using the non-repeater sample from Sand et al. (2024). The Spearman p -value is 0.005 (See Figure A3 in the Appendix), still larger than our significance threshold of 10^{-3} but smaller than that when examining the two samples separately.

It is possible that a significant portion of the DM from our sources is coming from the host galaxies and hence this obscures the correlation. However, for the three repeaters in Figure 1 at $DM > 700 \text{ pc cm}^{-3}$, host DMs of order 500 pc cm^{-3} would be needed to see the predicted negative DM-fluence correlation. While such a high host DM contribution has been seen for a handful of FRBs (Ocker et al. 2022b; Caleb et al. 2023), the average assumed DM host contribution is only $\sim 80_{-49}^{+69} - 90_{-19}^{+29} \text{ pc cm}^{-3}$ (Shin et al. 2023; Khrykin et al. 2024). One of these sources (FRB 20190417A) has a particularly large host RM (Mckinven et al. 2023a). However, the other two do not (Ng et al. in prep.; Mckinven et al. 2023a). Thus, large host DM contributions seems an unlikely explanation for all three sources. A more probable explanation is that repeating FRBs have a broad range of average intrinsic luminosities such that any correlation is undetectable.

4.1.5. Extragalactic DM & Scattering Correlation

Galactic pulsars show a strong correlation between their DM and scattering timescale (Bhat et al. 2004). A correlation between extragalactic DM and scattering for our FRBs could suggest that a significant portion of an FRB’s DM originates from the host galaxy, as the intergalactic medium (IGM) is expected to contribute negligible scattering (Ocker et al. 2022a).

In the left panel of Figure 2, we show the extragalactic (+halo) DM versus total scattering timescale for our repeating FRB sample. Most of the bursts in our sample do not have measured scattering timescales, and instead we place an upper limit on the scattering timescale equal to the width of the narrowest sub-component. As we will show in Section 4.3, we do not find evidence that the scattering time of a single repeating FRB changes with time. Hence, for each repeating source, we use (and show) either our scattering timescale with the smallest uncertainty or our most constraining upper limit.

Only 9 of the repeating FRB sources in our sample have at least one burst with a measured scattering timescale. Thus, the sample for this correlation is extremely limited. Nonetheless, the Spearman p -value us-

ing only the sources with measured scattering timescales is 0.63². We also run a censored Kendall τ test using the `cenken` function in R’s NADA package (Lopaka 2020; R Core Team 2020). The censored Kendall τ test allows us to account for upper limits on our scattering timescales (also referred to as left censored data). The Kendall τ value is 0.1, suggesting little to no correlation. The lack of a correlation supports the notion that a significant portion of the extragalactic DM does not arise from the same location as that of the scattering. Our results are similar to those of Sand et al. (2024).

4.2. Repeating vs. Non-repeating FRBs Morphology Comparison

We compare various morphological features between our sample of repeating FRBs and the thus-far non-repeating FRB sample presented by Sand et al. (2024). A significant advantage to comparing these two populations rather than including FRBs from instruments other than CHIME/FRB is that both suffer from the same instrumental biases, aside from their detection thresholds. The difference in detection thresholds is the most relevant for comparisons of the spectral fluences (F_ν) of the bursts. Thus, for all fluence comparisons, we only include bursts for which the real-time detection $S/N^3 > 20$. For other tests, we place cuts on the time resolution at which the burst is studied. Thus, this is approximately equivalent to a S/N cut, as only bursts with sufficient S/N can be studied at high time resolutions. We compare the bandwidth, total burst duration, number of burst components, sub-burst widths, sub-burst waiting times, and fluences between the two samples in Figures 2 - 6.

To assess the difference between the two populations, we use both the Anderson-Darling (AD; Anderson & Darling 1954) and Kolmogorov-Smirnov (KS; KST 2008) test statistics. Similar to in Section 4.1, we consider two samples to be distinct if the AD and KS test p -values are both $< 10^{-3}$. Results from all of our comparisons are listed in Table 1. We include the total number of repeating and non-repeating FRBs (or the number of bursts) used per comparison after applying various cuts in Table 1. We perform the comparisons using each individual burst from a given source, rather than the average of that quantity for the source. Thus, repeaters with a significant number of bursts will more heavily contribute to the given distributions.

² Given the low number of sources, and the low significance, we do not perform the same MC employed for previous correlations.

³ While the S/N threshold for non-repeaters is 12, we choose 20 to be well above the completeness level.

4.2.1. Extragalactic DM and Scattering for Repeating vs. Non-repeating Sources

CHIME/FRB Collaboration et al. (2023a) found a significant difference between the DM distributions of repeating and non-repeating FRBs. This DM distribution difference persisted as the S/N threshold of their sample was lowered, as well as when extragalactic DM instead of total DM was considered. They found an extragalactic DM difference of $161 \pm 55 \text{ pc cm}^{-3}$ between repeaters and non-repeaters detected above a S/N threshold of 12, with repeaters having on average lower extragalactic DMs. While our analysis has been able to refine the DM of repeating FRBs, the improvement has been on the order of $\sim 1 \text{ pc cm}^{-3}$ or less. Hence, we do not expect a significant change from the results of CHIME/FRB Collaboration et al. (2023a) regarding the DM distribution.

The difference in the DM distributions of the two samples could be due to either a) a difference in the host galaxy contributions or b) a difference in the distances to which we detect them (and hence the IGM contributions). However, unlike DM, the scattering contribution from the IGM is expected to be small (Macquart & Koay 2013; Ocker et al. 2022a). A difference in the scattering timescale distributions between the two samples would, in principle, provide direct evidence of different host environments for the two populations, or provide evidence that the IGM scattering contribution is significant. However, highly scattered, narrow bursts are harder to detect than highly scattered, wide bursts and so there is also a natural observational bias here.

The majority of the repeating FRBs in our sample do not show visible signs of scattering. However, we can still compare the scattering timescales (including upper limits) of our sample with those of non-repeating FRBs. In the left panel of Figure 2, we show the scattering timescale versus the extragalactic (+halo) DM for both repeating and non-repeating FRBs. Upper limits on the scattering timescales are shown with downward arrows.

To compare the two populations, we use the Kaplan-Meier method, a part of the python package `lifelines`, and the Peto-Peto test statistic (Peto & Peto 1972). These methods give significant advantages over the AD and KS tests as data can be labeled as either censored or uncensored. In the case of scattering timescales, the censored data are those for which we have only upper limits, while the uncensored data are the measured scattering timescales. In the right panel of Figure 2, we show the cumulative distribution function (CDF) of the repeating and non-repeating scattering distributions using the Kaplan-Meier method. The Peto-Peto test statistic for

Table 1. Comparisons between repeating and thus far non-repeating FRB parameters

Property	Cutoff	# Repeat bursts	# Non-repeat bursts	AD p -value ^a	KS p -value ^b
Bandwidth	N/A	118	125	< 0.001	3.4×10^{-24}
Duration	N/A	118	125	< 0.001	5.0×10^{-18}
Num. Components	$t_{\text{res}} \leq 0.16$ ms	20	79	0.25	0.99
Sub-burst Width	$t_{\text{res}} \leq 0.16$ ms	89 ^e	210 ^e	< 0.001	4.3×10^{-20}
Sub-burst Width	$t_{\text{res}} \leq 80\mu\text{s}$	36 ^e	190 ^e	< 0.001	1.2×10^{-6}
Sub-burst Width	$t_{\text{res}} \leq 40\mu\text{s}$	18 ^e	164 ^e	0.003	0.003
Duration-Normalized Sub-burst Width	$t_{\text{res}} \leq 0.16$ ms	89 ^e	210 ^e	0.24	0.15
Duration-Normalized Sub-burst Width	$t_{\text{res}} \leq 80\mu\text{s}$	36 ^e	190 ^e	0.015	0.0031
Duration-Normalized Sub-burst Width	$t_{\text{res}} \leq 40\mu\text{s}$	18 ^e	164 ^e	0.0032	0.0013
Wait time	$t_{\text{res}} \leq 0.16$ ms	48 ^f	113 ^f	< 0.001	8×10^{-19}
Wait time	$t_{\text{res}} \leq 80\mu\text{s}$	15 ^f	108 ^f	< 0.001	4×10^{-7}
Wait time	$t_{\text{res}} \leq 40\mu\text{s}$	6 ^f	98 ^f	0.01	0.01
Duration-Normalized Wait time	$t_{\text{res}} \leq 0.16$ ms	48 ^f	113 ^f	0.25	0.96
Duration-Normalized Wait time	$t_{\text{res}} \leq 80\mu\text{s}$	15 ^f	108 ^f	0.013	0.14
Duration-Normalized Wait time	$t_{\text{res}} \leq 40\mu\text{s}$	6	98	0.006	0.031
Fluence ^c	S/N > 20	35	50	0.04	0.12
Band-limited Fluence ^d	S/N > 20	35	48	0.25	0.48

^aAnderson-Darling test as implemented using `scipy.stats`. Note p -values are floored at 0.001.

^bKolmogorov-Smirnov test as implemented using `scipy.stats`.

^cSpectral fluence averaged over the entire CHIME/FRB 400-MHz band. We limit the sample bursts whose detection S/N is greater than 20.

^dSpectral fluence averaged over the spectral extent of the burst. We limit the sample to bursts whose detection S/N is greater than 20.

^eNumber of individual sub-bursts rather than number of detected bursts.

^fNumber of arrival time differences. Only applicable for multi-component bursts.

the two distributions is $p_{\text{PP}} = 1.0$. Thus, given the current sample sizes, there is no evidence for a difference in the scattering timescales of repeating and thus-far non-repeating FRBs. However, we caution that our repeating FRB sample is small, and those with measured scattering timescales even smaller. Additional repeating FRBs with measured scattering timescales could still reveal a difference between the two populations.

4.2.2. Burst Duration and Bandwidth for Repeating vs. Non-repeating Sources

Pleunis et al. (2021a) identified a difference in both the bandwidth and duration of repeating and non-repeating FRBs. Using ours and Sand et al. (2024)'s improved bandwidth and duration estimates, we compare the two in Figure 3. By eye, the two populations inhabit very different portions of the duration-bandwidth phase space, with repeating FRBs narrower in bandwidth and longer in duration than non-repeaters. We calculate

the AD and KS test values for bandwidth and duration separately and list them in Table 1. The full band was not recorded for a significant fraction of the non-repeating FRBs (see Sand et al. 2024, for a discussion of this). Thus, many of the bandwidths are lower limits. However, larger bandwidths for these sources would only increase the discrepancy seen between the two populations. The AD and KS test statistics provided in Table 1 assume that the bandwidth for these sources is equivalent to the lower limit. If we instead remove sources for which the bandwidth is a lower limit, the AD and KS test statistic for BW are $p_{\text{AD}} < 0.001$ and $p_{\text{KS}} = 4.5 \times 10^{-39}$. Thus, in both scenarios, this strongly indicates that the two populations are distinct in both BW and duration.

4.2.3. Sub-Burst Properties for Repeating vs. Non-repeating Sources

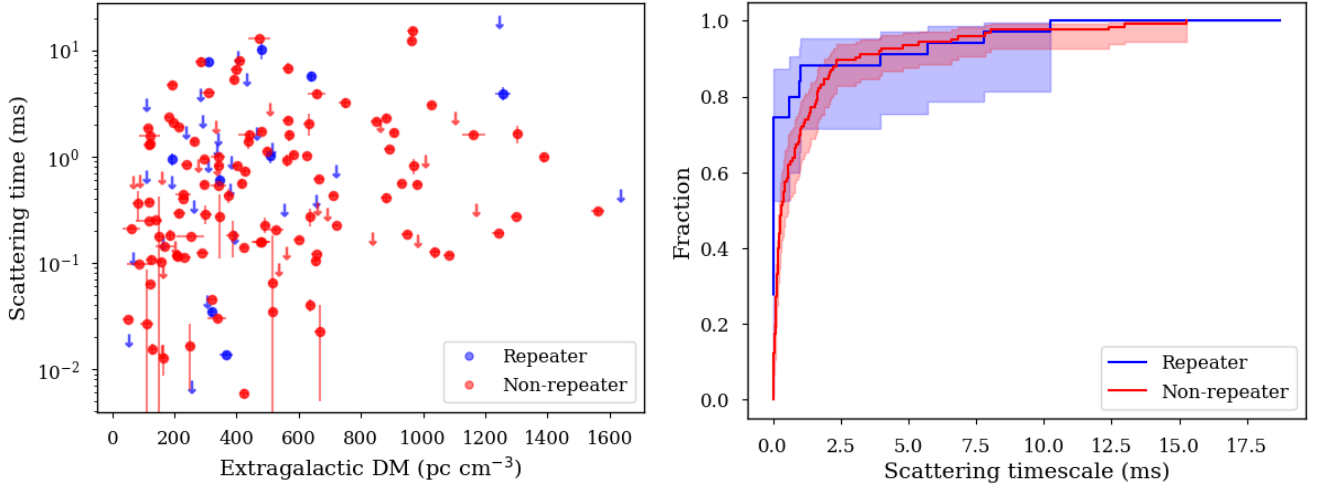


Figure 2. *Left panel:* Scattering versus extragalactic (+halo) DM for repeaters and non-repeaters. For DM, we subtract the Galactic component as determined using NE2001. Downward arrows represent upper limits on scattering timescales. For repeating FRBs, this is assumed to be the width of the narrowest sub-burst for that event. For non-repeating FRB parameter descriptions, see Sand et al. (2024). *Right panel:* Cumulative distribution function (CDF) for scattering for repeating and thus-far non-repeating FRBs using the Kaplan-Meier method for left-censored data.

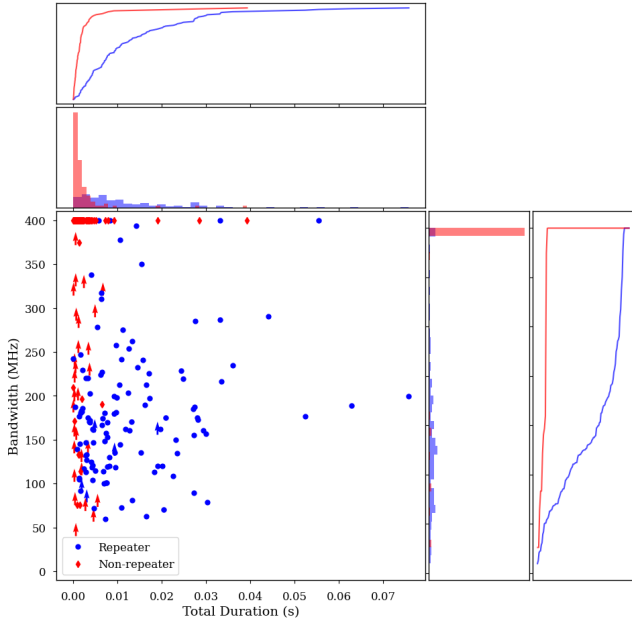


Figure 3. Bandwidth versus total duration for repeating and thus-far non-repeating FRBs. Bursts for which the full bandwidth was not available are indicated with arrows. Additionally, bursts for which the bandwidth is 400 MHz are again lower limits as this is solely set by the frequency range of CHIME. The normalized histograms and the cumulative distributions only include bursts for which the full bandwidth was recorded.

In an effort to systematically search for other apparent differences in emission phenomenology between

repeaters and non-repeaters, we compare the number

of sub-bursts per event⁴, the width of individual sub-bursts, and the waiting time (defined as the difference in the time of arrival of individual sub-bursts) between the two populations. However, all of these comparisons can be biased by the time resolution at which we study the populations as additional components may be unresolved at lower resolutions. To try to address this bias, we limit the comparison to bursts (both repeating and non-repeating) studied at a time resolution ≤ 0.16 ms. However, a bias may still remain as many of the non-repeating FRBs are bright enough to be analyzed at time resolutions ≤ 20.48 μ s (e.g., 51 out of 125 bursts) while only 7 bursts from our repeating sample are studied at time resolutions ≤ 20.48 μ s. Additionally, we note that more active repeaters will influence the distributions more than less active sources, as we use every burst from each source with the required data for our comparisons.

Nonetheless, there are 94 bursts (210 sub-bursts) from non-repeating FRBs and 40 bursts (89 sub-bursts) from repeating FRBs that we analyze at a time resolution ≤ 0.16 ms. In Figure 4 we compare the number of sub-burst components, the sub-burst widths, and the waiting time of sub-bursts between the two populations. The

⁴ Note this is not per source, but rather per individual burst from a given source.

AD and KS test statistics for each comparison is listed in Table 1.

While the number of sub-bursts is consistent between the two populations, the sub-bursts widths and waiting times are not (Figure 4). The average width of an individual sub-burst for repeaters is 2.7 ms while that for non-repeaters is 0.57 ms. Additionally, the average wait time for repeaters is 5.2 ms while that for non-repeaters is 1.2 ms. We re-do our analysis only using bursts studied at even higher time resolutions (e.g., $\leq 81.92 \mu\text{s}$ and $\leq 40.96 \mu\text{s}$) The p -values for the smaller samples are larger, suggesting that the sub-burst width and waiting time differences may not be inherent to the two populations and instead are solely due to missed components at lower time resolutions (see Figure A4 in the Appendix). However, we note the sample of repeating FRBs at resolutions $\leq 40.96 \mu\text{s}$ is very small, and may simply be insufficient to reject the null hypothesis that the two samples originate from the same distributions.

Given that repeating FRBs have longer durations than non-repeaters, we explore whether the duration-normalized sub-burst and waiting times between the two populations are consistent. In Figure 4, we show the duration-normalized sub-burst width and waiting times for the larger burst sample (e.g., bursts studied at time resolutions ≤ 0.16 ms). Interestingly, the AD and KS test-statistics for both duration-normalized sub-burst width and duration-normalized waiting times are not significant. We also re-do the comparison excluding single component bursts for which the duration-normalized individual sub-burst width would be 1. This new sample consists of 165 non-repeater sub-bursts and 72 repeater-sub-bursts. The p -values are slightly smaller but still significantly above 10^{-3} .

We also re-do our analysis with even higher time resolution limits (e.g., $81.92 \mu\text{s}$ and $40.96 \mu\text{s}$). The p -values for the duration-normalized wait times and widths are now slightly smaller, but still greater than 10^{-3} (see Figure A4 in the Appendix).

In Figure 5, we show sub-burst width versus total duration for all repeating and non-repeating bursts in our sample studied at time resolutions ≤ 0.16 ms. We exclude bursts for which there is only one component, as these would cluster along a 1:1 line. There is a positive correlation between sub-burst width and total burst duration. This suggests that there may be a shared physical scaling for repeating and non-repeating FRBs relating to their total widths and sub-burst widths. Additional repeating FRBs studied at the highest time resolutions will provide further insight into this new finding.

4.2.4. Spectral Fluences for Repeating vs. Non-repeating Sources

There is an inherent bias in a comparison of the spectral fluences⁵ of the two populations since the triggering threshold at CHIME/FRB for the complex raw voltages is lower for repeaters than for non-repeaters. Thus, we only include bursts in our sample for which the initial detection S/N was > 20 , as this is sufficiently above the triggering threshold for both repeating and non-repeating sources. Additionally, missing channels due to RFI masking could also affect this comparison. However, given we are only comparing bursts detected by CHIME, we do not expect drastic changes in the total fraction of the band that is masked due to RFI. We remove bursts for which the top available channel was less than 800 MHz, though (e.g., those for which $\text{DM} > 1000 \text{ pc cm}^{-3}$).

With the S/N cut of 20, the AD and KS test statistics do not suggest the two are drawn from different distributions. However, repeaters have on-average lower spectral fluences than non-repeaters (17 Jy ms versus 91 Jy ms, respectively; see left panel of Figure 6). This is expected as repeating FRBs are on average more narrow-band than non-repeating FRBs, and thus their spectral fluences over the entire CHIME/FRB bandwidth will be lower than those of a broadband non-repeater as more noise is averaged in. To alleviate this, we re-calculate each burst's spectral fluence solely over the spectral extent of that burst. We compare this new, band-limited spectral fluence for repeating and non-repeating FRBs in the right panel of Figure 6. We again limit our sample to bursts detected with a real-time S/N > 20 . The two are consistent with being drawn from the same distribution, with the AD and KS test values listed in Table 1. If we again re-do this analysis but with a real-time S/N limit of > 15 , the two remain consistent with being drawn from the same distribution.

CHIME/FRB's detection algorithm uses a boxcar matched filter that effectively integrates over the burst in frequency and time. Thus, a non-repeating FRB with a larger bandwidth yet the same band-limited fluence as a repeating FRB should have a higher detection S/N. We note, however, that there are a few instances in which this does not occur. Significant frequency-dependent noise weighting or RFI flagging can boost a narrowband signal's S/N. Additionally, CHIME/FRB's detection algorithm searches over two spectral indices, such that a narrowband burst at the top or bottom of the band can again be boosted in S/N.

⁵ Unless specified otherwise, the spectral fluences referred to throughout this work will be those averaged over the full 400 to 800 MHz CHIME/FRB band.

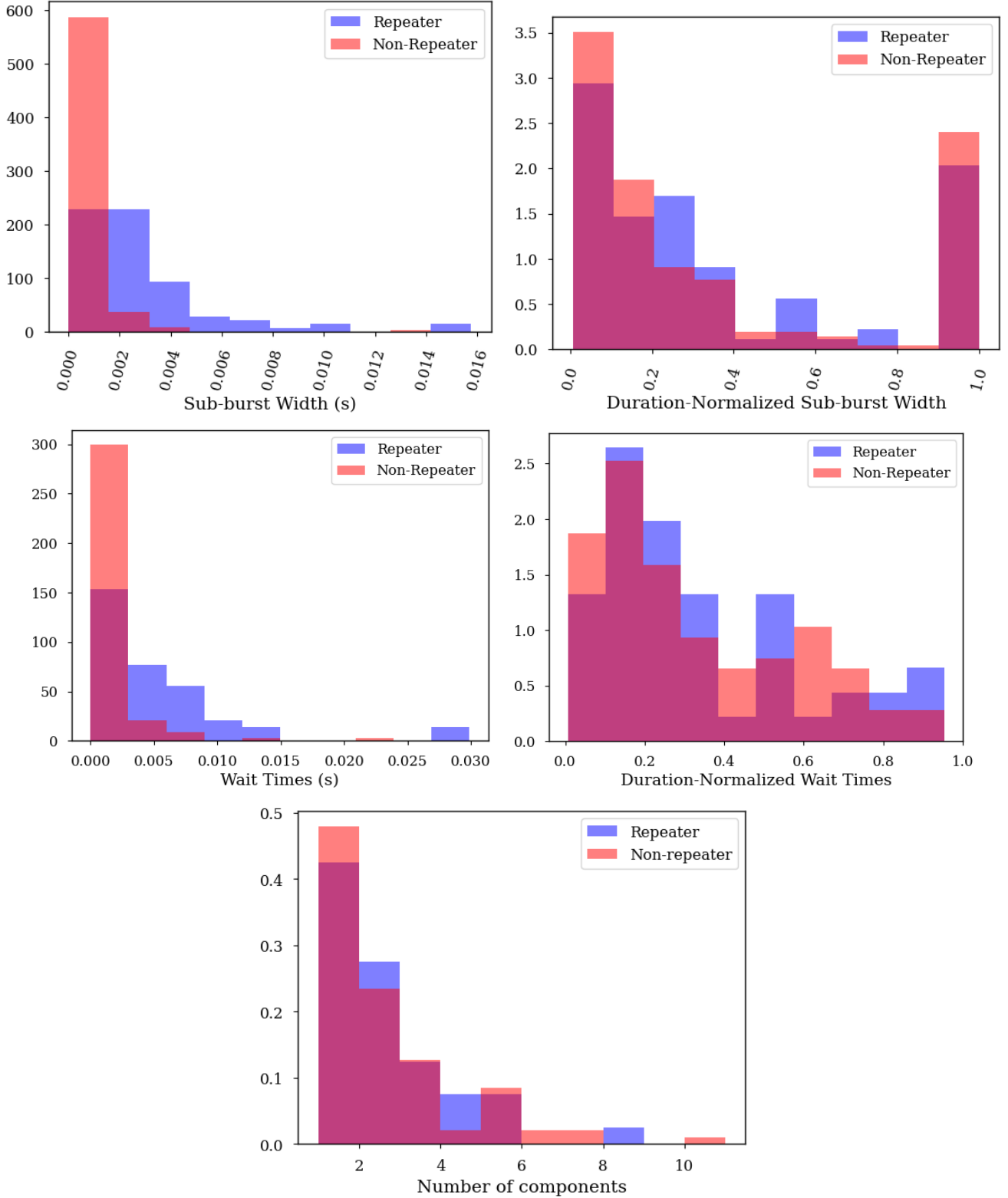


Figure 4. *Left top panel:* Sub-burst width distribution for repeating and thus-far non-repeating FRBs. We limit the two samples to only include bursts studied a time resolution ≤ 0.16 ms. *Right top panel:* Same as left panel except for the sub-burst width normalized by the total burst duration. *Left middle panel:* Wait time distribution for repeating and thus far non-repeating FRBs. The wait time is defined as the difference in arrival time between subsequent sub-bursts for a given FRB. The sample is limited to bursts which were analyzed at time resolutions equal to or less than 0.16 ms. *Right middle panel:* Same as the left panel except the duration-normalized wait time. Each wait time is normalized by the total duration of that given burst. *Bottom panel:* Number of sub-burst components for repeating and thus-far non-repeating FRBs. We limit the two samples to only include bursts studied a time resolution ≤ 0.16 ms.

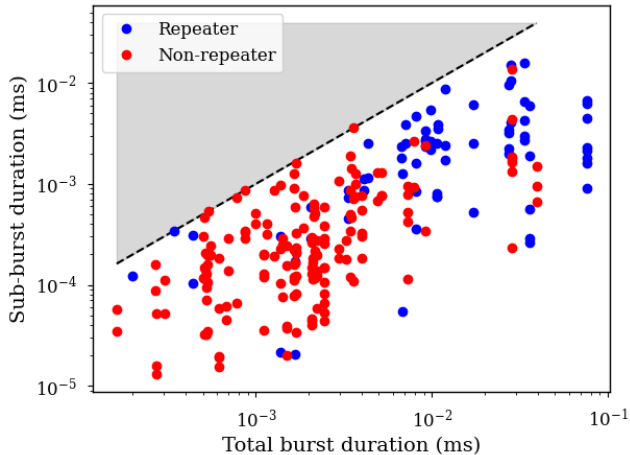


Figure 5. Sub-burst width versus total burst duration for all repeating and non-repeating bursts studied at time resolutions ≤ 0.16 ms. We do not include bursts for which there is only one component. The grey shaded region indicates an unphysical phase space where the sub-burst width would be larger than the total burst duration.

Nonetheless, in most cases, a broadband burst with the same specific fluence should have a larger S/N than a narrowband burst. Thus, we should be able to detect broadband non-repeating FRBs out to larger distances than narrowband repeaters. This is consistent with the differences seen in the DM distribution for repeating and thus far one-off FRBs (CHIME/FRB Collaboration et al. 2023a). However, for the spectral fluence over the spectral extent of the bursts to be consistent between the two populations, this would imply that non-repeaters have, on-average, intrinsically higher specific energies than repeating FRBs.

To test the hypothesis that an FRB with the same band limited spectral fluence should have a higher detection S/N for a larger bandwidth, we investigate the detection S/N versus bandwidth for our repeating sources (see Figure A5 in the Appendix). However, we cannot draw any significant conclusions due to the large range of spectral fluences exhibited by a single source along with the small bandwidth ranges. Future injections of bursts to better understand CHIME/FRB’s detection sensitivity should lend significant insights into this.

4.3. Spectral Fluence, Bandwidth, DM, and Scattering Time Variations

If FRBs are young NS embedded in turbulent environments, we might expect the local environment (probed through the DM, rotation measure, scattering timescale, and scintillation features) of these sources to change

with time (Piro & Gaensler 2018).⁶ Michilli et al. (2018) found extreme changes in the rotation measure (RM) of FRB 20121102A (which may be embedded in a young nebula e.g., see Marcote et al. 2017) while Hessels et al. (2019) found evidence for DM changes of $\sim 1\text{-}4$ pc cm $^{-3}$ over a four year period for this source. Mckinven et al. (2023b) and Ng et al. (in prep.) also both find that most repeating FRBs show subtle RM changes of order a few rad m $^{-2}$, while some show significant RM variations. However, Mckinven et al. (2023b) did not perform detailed studies of the DMs of the sources in their analysis. Bethapudi et al. (2022) also found changes in the scintillation bandwidth for FRB 20180916B with time.

Here, we explore whether any sources in our sample show changes in their DM and scattering timescale as a function of time. In particular, we focus on the repeating sources FRB 20191106C, FRB 20200929C, FRB 20181119A, FRB 20190208A, FRB 20190303A, and FRB 20190417A. These sources are chosen as they each have six or more bursts with the complex raw voltages recorded⁷. In addition to DM and scattering timescales, we also explore whether the spectral fluence of a burst impacts (or is impacted by) any other burst property and whether there is a systematic change in the emitting bandwidth of these sources (largely motivated by FRB 20180916B, whose activity window is frequency dependent e.g., see Pastor-Marazuela et al. 2021; Pleunis et al. 2021b; Bethapudi et al. 2022). To quantify changes in a given parameter, we perform a weighted least-squares fit assuming a linear function. We do not include bursts for which we either calculate an upper limit on the scattering timescale, or for which we do not report a DM uncertainty.

In Figures 7 - 12, we show the fluence, DM, scattering timescale (if applicable⁸), and frequency range for FRBs 20181119A, 20190208A, 20190303A, 20190417A, 20191106C, and 20200929C, respectively. The best-fit slopes for spectral fluence, DM, and scattering timescale (along with their 1σ uncertainties) are listed in Table 2. Except for the temporal variation of the spectral fluence of FRB 20181119A, all other derived slopes are either not statistically significant or are due to underestimated measurement uncertainties. We do not perform

⁶ We note, however, that changes in the DM, rotation measure, etc. could also be caused by the relative motion of the source with respect to us and thus a changing DM does not directly imply a changing environment.

⁷ A minimum of six bursts was chosen in order to have a sufficiently large sample of burst property measurements while also enabling examination of multiple sources from our sample.

⁸ Only shown if we can measure a scattering timescale for at least one of the bursts from the source.

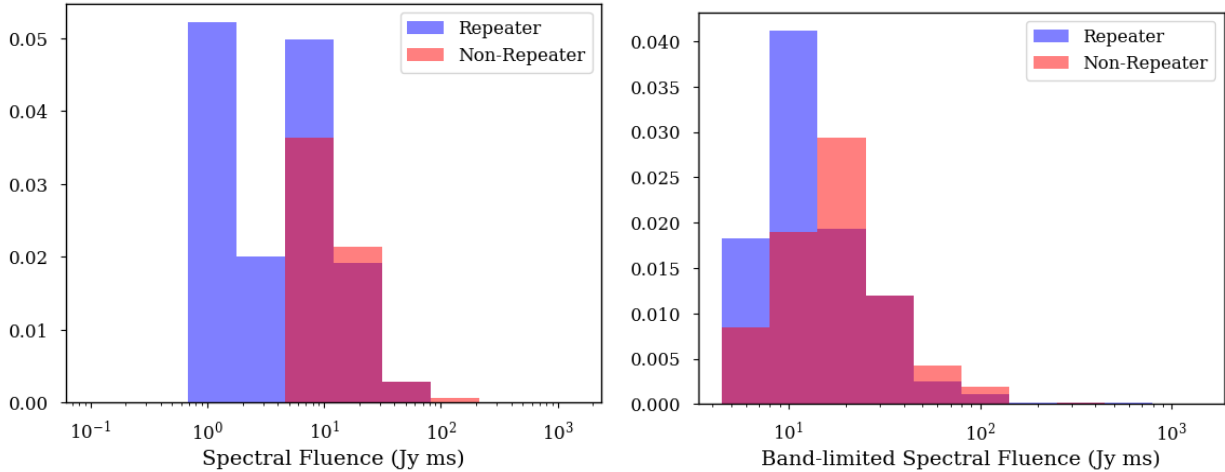


Figure 6. *Left panel:* Band-averaged spectral fluence distribution for repeating and thus-far non-repeating FRBs over the entire 400-MHz CHIME/FRB bandwidth. As repeating FRBs have a different threshold for triggering the complex raw voltages than non-repeaters at CHIME/FRB, we limit the sample to bursts (repeating & non-repeating) whose detection S/N is greater than 20. We also only include bursts for which the full CHIME/FRB band was recorded. *Right panel:* Same as left panel except a band-limited spectral fluence calculation in which the spectral fluence is only determined over the frequency channels that contain emission from the source.

the same comparison for bandwidth, as the central frequency is highly dependent on the CHIME/FRB beam response which we have not corrected for in this work. Thus, for bandwidth, only by-eye trends are reported⁹.

4.3.1. Spectral Fluence Variations over Time

FRB 20181119A is the only source for which there is a significant (slope greater than the 3σ uncertainties) change in the spectral fluence (over the entire 400-MHz CHIME/FRB band) with time (see Figure 7). The best fit slope is -1.2 ± 0.2 Jy ms yr⁻¹.

4.3.2. Bandwidth Variations over Time

No sources in our sample show any systematic, significant trend of frequency range with time. Sheikh et al. (2024) found a decrease in both the central frequency and bandwidth of FRB 20220912A over an approximately two month observational period. However, there was significant scatter in their measurements, and given our small sample size per source, it is possible that such a correlation is not yet obvious. Additionally, as we have not corrected for the primary beam effects of CHIME for individual source spectra, we do not perform an analysis of the central frequency as a function of time, as these measurements would be highly biased by beam effects.

⁹ The actual bandwidths are still calculated using the `fitburst` model assuming a running power law.

4.3.3. DM Variations over Time

Determining the DM for a given burst using `fitburst` is particularly difficult for repeating FRBs due to both the complex frequency and time structure displayed and the (on average) low S/N of these bursts. Thus, for our DM comparisons, we instead use the DM determined using the `DM phase` routine (Seymour et al. 2019) as we found that it visually performed better for our sample. Unlike `fitburst` which fits a set of modified Gaussians to the data, `DM phase` maximizes the structure of the burst and is significantly more indifferent to the intrinsic shape of the data than `fitburst`. Thus, for highly complex bursts, the `DM phase` package often better visually aligns a burst.

Other than FRB 20181119A (Figure 7), none of the sources in our sample have a significant secular increase or decrease in DM as a function of time. While the trend for FRB 20181119A is significant, it is based on only three data points, and does not include the final two measurements that were estimated by-eye. Additionally, we manually de-disperse all bursts from this source to the weighted-average DM and all bursts still appear fully de-dispersed. Thus, the variation for this source is likely not astrophysical and is instead due to difficulty in determining the DMs of the bursts as many have low S/Ns without obvious sub-structure.

FRB 20190208A also shows significant variation about the mean DM. However, we de-disperse the three outlier bursts to the average DM and all appear fully de-dispersed. Thus, similar to FRB 20181119A, the variation is likely not astrophysical but solely due to our in-

Table 2. Individual Source Parameter Variations with Time

Source	Spectral Fluence (Jy ms yr ⁻¹)	DM (pc cm ⁻³ yr ⁻¹)	Scat. Time (ms yr ⁻¹)
FRB 20181119A	-1.2 ± 0.2	1.3 ± 0.3	-
FRB 20190208A	-0.001 ± 0.9	0.1 ± 0.07	-
FRB 20190303A	-0.7 ± 0.4	-0.04 ± 0.02	-0.2 ± 0.07
FRB 20190417A	-1.8 ± 2.5	-0.09 ± 0.6	0.1 ± 0.2
FRB 20191106C	14 ± 6	1 ± 2	-1.5 + / - 0.6
FRB 20200929C	9 ± 5	-0.3 ± 0.06	-

ability to determine precise DMs for certain bursts. The DMs for the remaining sources (FRB 20190303A, FRB 20190417A, FRB 20191106C, and FRB 20200929C) show small variations, but most are still consistent with the respective inverse-variance weighted DM within uncertainties.

4.4. Scattering Timescale Variations over Time

The measured scattering timescale per burst is determined using the 2D spectro-temporal fit from `fitburst`. Due to the degeneracy between scattering and downward drifting, we only report scattering timescales for bursts for which we can see by-eye evidence for scattering. We do not find evidence for a secular change in the scattering timescales of FRB 20190303A (Figure 9), FRB 20190417A (Figure 10), or FRB 20191106C (Figure 11). All of our measured scattering timescales for the two FRBs with scattering upper limits, FRB 20190208A (Figure 8) and FRB 20190303A (Figure 9), are consistent with the scattering times that we report for the sources.

5. DISCUSSION

5.1. Local Environments

For the six repeating FRBs presented in Section 4.3, we do not find evidence for significant changes in scattering or DM variations with time. Long-term monitoring of other highly active sources such as FRB 20180916B (Sand et al. 2023), FRB 20201124A (Lanman et al. 2022), and FRB 20220912A (Konijn et al. 2024) have also not yet shown any significant DM variations with time, although they found low-level (~ 1 pc cm⁻³), short timescale DM variations. While this might suggest that most FRBs do not lie in environments similar to that of FRB 20121102A (Michilli et al. 2018; Hessels et al. 2019), the total sample of repeaters for which possible DM variations have been studied remains small. Additionally, possible changes in the DM due to a putative expanding supernova shell are highly dependent on the

age of the remnant, with certain periods having little to no change in the DM (Piro & Gaensler 2018).

Petroff et al. (2013) searched for systematic DM variations in 168 Galactic radio pulsars, and found that only four showed significant variations of order 0.005 to 0.2 pc cm⁻³ yr⁻¹. They attributed these DM variations to either an associated pulsar wind nebulae/supernova remnant or a turbulent ISM. However, these variations are significantly below the constraints placed here. Desvignes et al. (2018) also searched for a systematic DM variation in the Galactic centre magnetar, PSR J1745–2900. They found a decline of ~ 10 pc cm⁻³ over a period of four years. However, their results were consistent with no secular change within 2σ .

As discussed in Section 4.2, we do not find a statistical difference in the scattering timescales between repeating and non-repeating FRBs. Pandhi et al. (2024) found no significant difference in the linear polarization fraction or the extragalactic RM when comparing these two populations. They did not, however, find any thus-far non-repeaters with extreme RMs, in contrast with the extreme RMs seen in the repeating FRBs 20121102 and 20190520B (Michilli et al. 2018; Anna-Thomas et al. 2023). This could be explained by intra-channel depolarization in the CHIME/FRB band, though. Nonetheless, taken together, these findings suggest that repeating and non-repeating FRBs share similar local environments. This supports the notion that the differences observed in the DM distributions by CHIME/FRB Collaboration et al. (2023a) are unlikely to be driven by local environmental factors. Nonetheless, the small number of known repeating FRBs compared to non-repeaters suggests that these conclusions should be viewed cautiously, as additional data may reveal more subtle differences.

5.2. Luminosity

Similar to the results of Sand et al. (2024), we do not find a correlation between extragalactic (+halo) DM and fluence for our repeating FRB sources. As seen in

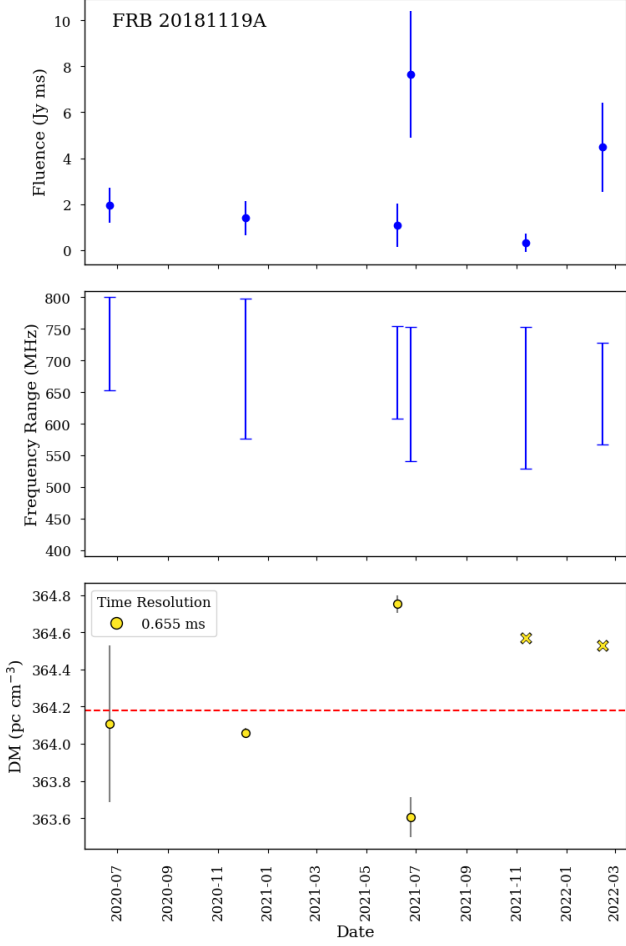


Figure 7. Band-averaged fluence (calculated over the entire CHIME/FRB bandwidth), CHIME/FRB frequency range, and DM for FRB 20181119A as a function of time. Error bars for fluence and DM are shown at the 99% confidence level. The time resolution at which the burst is analyzed is shown by the color of the points. The lowest time resolution is 0.655 ms while the highest is 2.56 μ s. For this source, all bursts were analyzed at a time resolution of 0.655 ms, so no variation is seen in the color. We note that the uncertainties for bursts studied at a time resolution of 0.655 ms may be underestimated due to the inability to discern structure at such a low time resolution. For this source, all bursts were analyzed at 0.655 ms, hence the same color for all points. For the DM, we show the inverse-variance weighted average as a red line. Bursts for which we could not calculate an optimal structure-maximized DM, and hence for which a by-eye DM was estimated, are shown as crosses. By-eye DMs were only estimated to within ~ 0.5 pc cm^{-3}

Figure 1, a single source can emit bursts with fluences ranging from 10^{-2} to 10 Jy ms. This is similar to FRB 20201124A, which exhibits fluence values spanning five orders of magnitude (Xu et al. 2022; Kirsten et al. 2024) and to SGR 1935+2154, which also emits bursts spanning ~ 7 orders of magnitude (Kirsten et al. 2021). To-

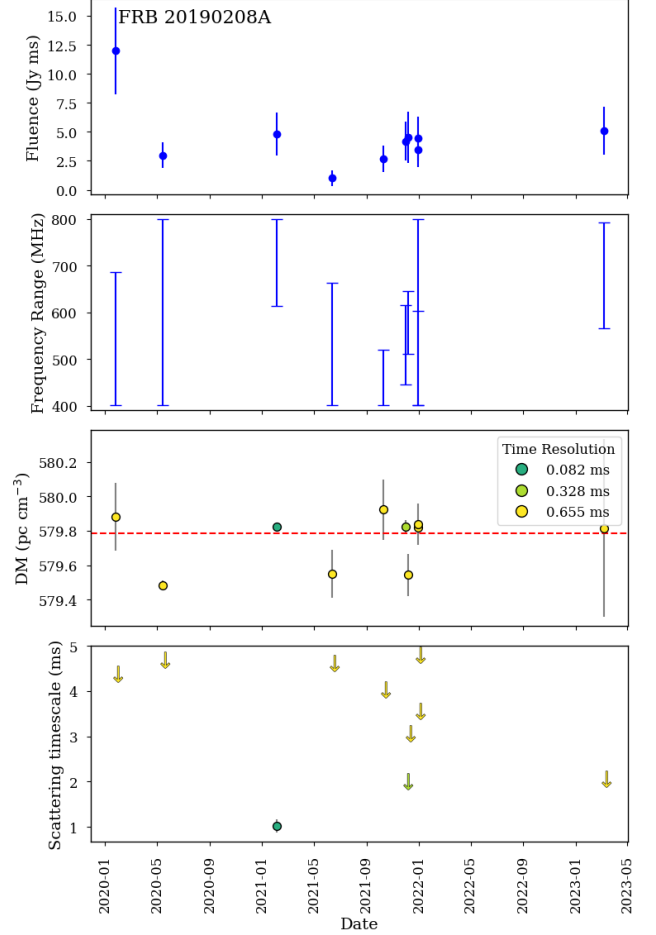


Figure 8. Same as Figure 7 except for FRB 20190208A. As FRB 20190208A has at least one burst with a measured scattering timescale, we also include the scattering timescale. For bursts for which there was no by-eye visible scattering timescale, we determine an upper limit on the scattering timescale as equivalent to the reported width of the narrowest sub-burst.

gether, this suggests that FRBs have broad luminosity distributions.

5.3. Multiple FRB Classes?

Our work further supports the results of Pleunis et al. (2021a) and Sand et al. (2024) who find clear morphological distinctions between repeating and thus-far non-repeating FRBs. Repeating FRBs tend to be narrower in bandwidth and longer in total duration than non-repeating FRBs (see Figure 3). We also find differences between the band-averaged fluences, sub-burst durations, and sub-burst waiting times of the two populations. Interestingly, when we normalize the sub-burst durations and waiting times of the two populations by the respective burst’s total duration, the distributions are consistent with being drawn from the same popula-

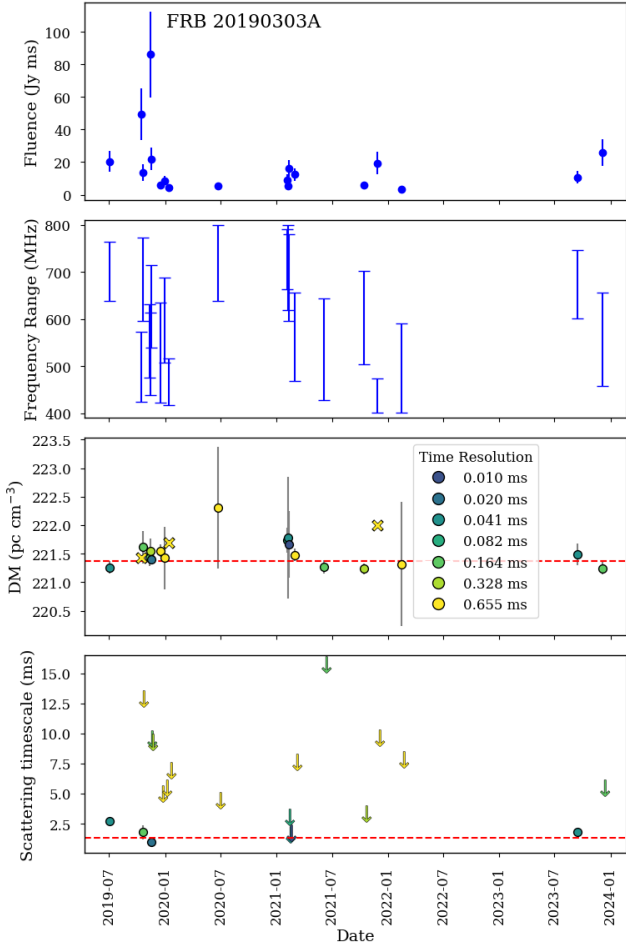


Figure 9. Same as Figure 8 except for FRB 20190303A. We do not include an extreme outlier burst for which the fluence was 351 Jy ms on 2021-06-06.

tion (see Figure 4). This could hint at a similar physical mechanism for the scaling of sub-burst width to the common envelope. However, we caution that for the repeating FRB population, we may be missing additional sub-bursts as most bursts were not studied at as high of a time resolution as the non-repeating sample. A larger number of repeating sources studied at microsecond time resolutions should provide further insight into this.

The band-averaged fluences over the burst spectral extents for the two populations are consistent with being drawn from the same distribution. Given that CHIME/FRB Collaboration et al. (2023a) found a significant difference between the DM distributions of the two samples, along with the larger bandwidths of non-repeaters, this could suggest a difference in their intrinsic specific energies. One possible interpretation is that repeaters and non-repeaters are produced by the same populations of physical object with non-repeaters the

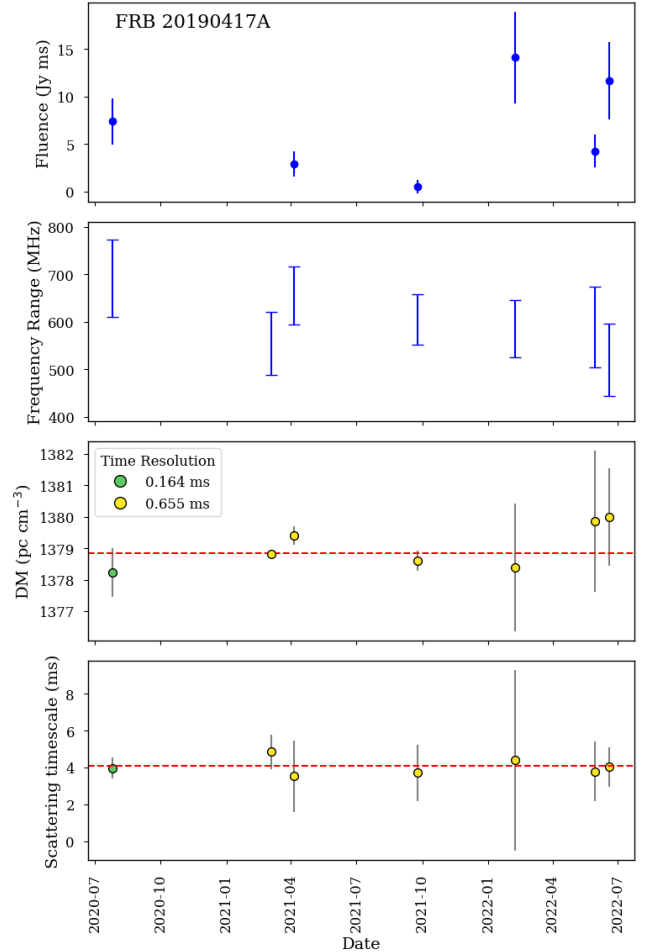


Figure 10. Same as Figure 8 except for FRB 20190417A

brightest bursts from a given repeater, primarily due to their larger bandwidths but also due to higher specific energies.

Kirsten et al. (2024) found that the energy-distribution for the high-energy bursts from FRB 20201124A was consistent with that of non-repeaters, similarly suggesting that non-repeaters might be the brightest burst from a repeater. Most recently, Ould-Boukattine et al. (2024) found similar results for FRB 20220912A. However, Kirsten et al. (2024) did not find any significant morphological or spectral differences between the high-energy bursts from FRB 20201124A and the lower-energy bursts. This could be in-part due to their comparatively smaller bandwidth. We also did not find any distinct morphological differences between the brightest bursts from our sources and the other bursts from the same source. A larger population of bright, repeating sources detected over large bandwidths is needed to explore this in further detail.

6. SUMMARY AND FUTURE WORK

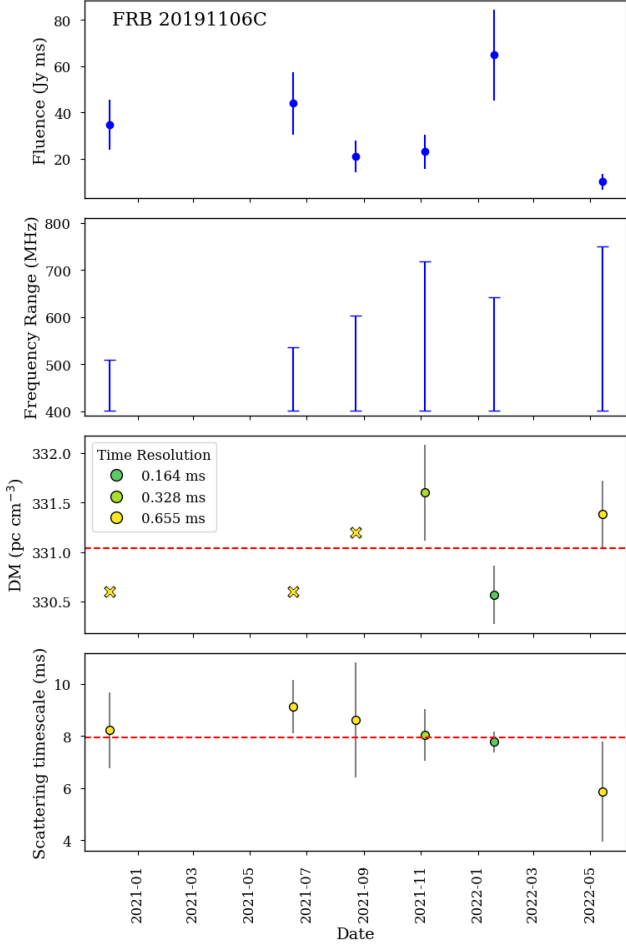


Figure 11. Same as Figure 8 except for FRB 20191106C.

In this work, we present for the first time a morphological analysis of the raw voltage data for 118 bursts from 32 unique repeating sources detected by CHIME/FRB. We present spectro-temporal fits for each burst at timescales down to microseconds, along with improved flux and fluence measurements for each burst. We search for correlations amongst the burst fluences, DMs, burst rate, and burst duration. We do not find any significant correlations amongst these parameters, even with improved fluences, burst rates, and burst duration estimates. The lack of a correlation between fluence and extragalactic DM (+MW halo) for our sources suggests that repeating FRBs have intrinsically large luminosity ranges. Additionally, the lack of a correlation between burst rate and total duration may suggest that that burst widths are not correlated with their beaming angle. We also search for an extragalactic DM (+MW halo) and scattering correlation, but again do not find one. A lack of a correlation suggests that the medium responsible for the majority of the extragalactic DM is

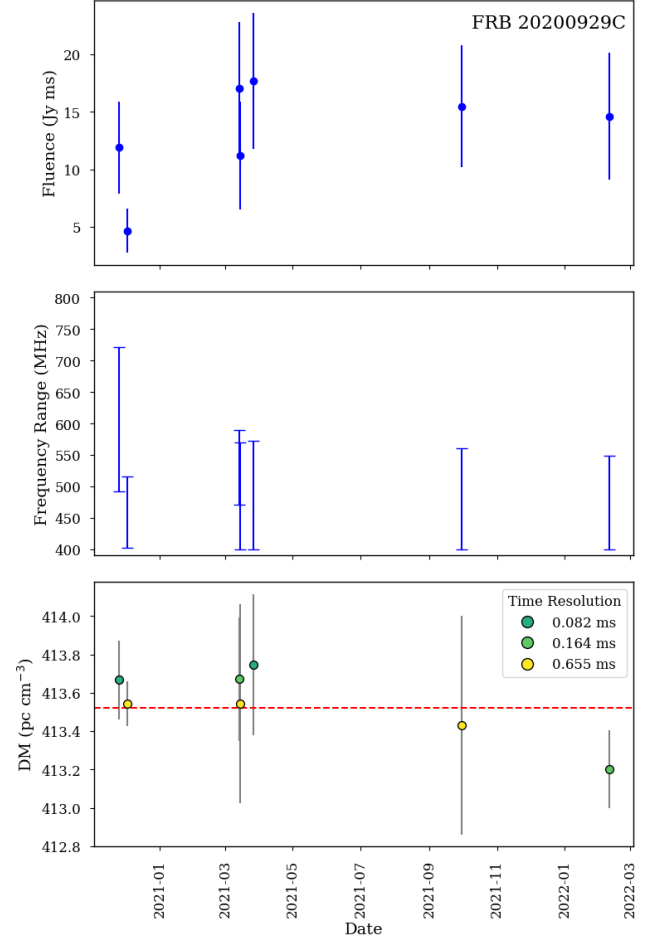


Figure 12. Same as Figure 7 except for FRB 20200929C.

not the same which primarily contributes to the sources scattering timescales.

We perform the first large-scale comparison of the morphology of the repeating and non-repeating FRB populations at timescales down to microseconds. Using the non-repeating FRB sample presented in Sand et al. (2024), we confirm the results of Pleunis et al. (2021a) that non-repeating FRBs have, on average, larger bandwidths and shorter temporal durations than repeating sources. Additionally, with increased time resolution, we compare the sub-burst properties of the two populations. Our results suggest that their may be a common duration normalized sub-burst duration amongst the two populations. Additionally, we find that the spectral fluences of the two populations over their spectral extents are consistent with being draw from the same distribution, despite non-repeating FRBs having larger bandwidths and, on average, larger DMs. This suggests that non-repeating FRBs may have intrinsically higher specific energies than repeating FRBs.

We also do not find a significant difference in the scattering timescales of the two populations. In combination with the work of Pandhi et al. (2024), this suggests that repeating and non-repeating FRBs do not generally have different local environments. However, the repeating FRB sample size for this comparison is low, and hence we caution strong interpretations of this result.

Lastly, we examine the temporal variations of spectral fluence, bandwidth, DM, and scattering for six of the FRB sources in our sample. Only one source, FRB 20181119A, shows a significant trend in its fluence as a function of time, with a rate of $-1.2 \pm 0.2 \text{ Jy ms yr}^{-1}$. None of our sources show secular increases/decreases in the DM and scattering timescales, constrained to $\lesssim 1 \text{ pc cm}^{-3} \text{ yr}^{-1}$ and $\lesssim 2 \text{ ms yr}^{-1}$, respectively.

CHIME/FRB, with its daily view of the sky north of $\delta = -11^\circ$, excels at finding repeating FRBs. The prospects for increasing the size of the known repeater population in the coming years is therefore excellent and will enable future similar studies with greater statistics. Additionally, with the upcoming CHIME/FRB Outrigger telescopes (Lanman et al. 2024), sub-arcsecond localizations will be available for most events, enabling host galaxy and redshift determinations, which will greatly aid many property comparisons and may eventually allow important correlations to emerge.

ACKNOWLEDGMENTS

We acknowledge that CHIME is located on the traditional, ancestral, and unceded territory of the Syilx/Okanagan people. We are grateful to the staff of the Dominion Radio Astrophysical Observatory, which is operated by the National Research Council of Canada. CHIME is funded by a grant from the Canada Foundation for Innovation (CFI) 2012 Leading Edge Fund (Project 31170) and by contributions from the provinces of British Columbia, Québec and Ontario. The CHIME/FRB Project, which enabled development in common with the CHIME/Pulsar instrument, is funded by a grant from the CFI 2015 Innovation Fund (Project 33213) and by contributions from the provinces of British Columbia and Québec, and by the Dunlap Institute for Astronomy and Astrophysics at the University of Toronto. Additional support was pro-

vided by the Canadian Institute for Advanced Research (CIFAR), McGill University and the McGill Space Institute thanks to the Trottier Family Foundation, and the University of British Columbia. The CHIME/Pulsar instrument hardware was funded by NSERC RTI-1 grant EQPEQ 458893-2014.

A.P.C is a Vanier Canada Graduate Scholar K.R.S. acknowledges support from Fonds de Recherche du Québec – Nature et Technologies (FRQNT) Doctoral Research Award Z.P. is supported by an NWO Veni fellowship (VI.Veni.222.295). V.M.K. holds the Lorne Trottier Chair in Astrophysics & Cosmology, a Distinguished James McGill Professorship, and receives support from an NSERC Discovery grant (RGPIN 228738-13). E.F. is supported by the National Science Foundation grant AST-2407399. K.S. is supported by the NSF Graduate Research Fellowship Program. K.N. is an MIT Kavli Fellow. F.A.D is supported by a Jansky Fellowship G.M.E. holds a Collaborative Research Team grant from the Canadian Statistical Sciences Institute (CANSSI), which is supported by Natural Sciences and Engineering Research Council of Canada (NSERC), and an NSERC Discovery Grant RGPIN2020-04554. A.H.M. is supported by a Collaborative Research Team grant from the Canadian Statistical Sciences Institute (CANSSI) C. L. is supported by NASA through the NASA Hubble Fellowship grant HST-HF2-51536.001-A awarded by the Space Telescope Science Institute, which is operated by the Association of Universities for Research in Astronomy, Inc., under NASA contract NAS5-26555. K.W.M. holds the Adam J. Burgasser Chair in Astrophysics. A.P. is funded by the NSERC Canada Graduate Scholarships – Doctoral program. A.B.P. is a Banting Fellow, a McGill Space Institute (MSI) Fellow, and a Fonds de Recherche du Québec – Nature et Technologies (FRQNT) postdoctoral fellow. M.W.S. acknowledges support from the Trottier Space Institute Fellowship program. P.S. acknowledges the support of an NSERC Discovery Grant (RGPIN-2024-06266). FRB research at UBC is funded by an NSERC Discovery Grant and by the Canadian Institute for Advanced Research. The baseband recording system on CHIME/FRB is funded in part by a CFI John R. Evans Leaders Fund award to IHs.

APPENDIX

Below, in Figure A1, we include the waterfall plots for a sub-sample of the bursts analyzed in this work. In Table A1, we include the measured burst parameters for each burst. In Figure A3, we show the fluence versus extragalactic DM (+halo) correlation including non-

repeating FRBs from Sand et al. (2024). In Figure A4, we show comparisons of the repeating and non-repeating sample, but limit the sample to bursts studied at time resolutions $\leq 40 \mu\text{s}$. In Figure A5 we show the bandwidth versus detection S/N for all sources in our sample

for which there are more than five bursts. Lastly, in Table A2, we list updated burst rates for the repeaters in our sample.

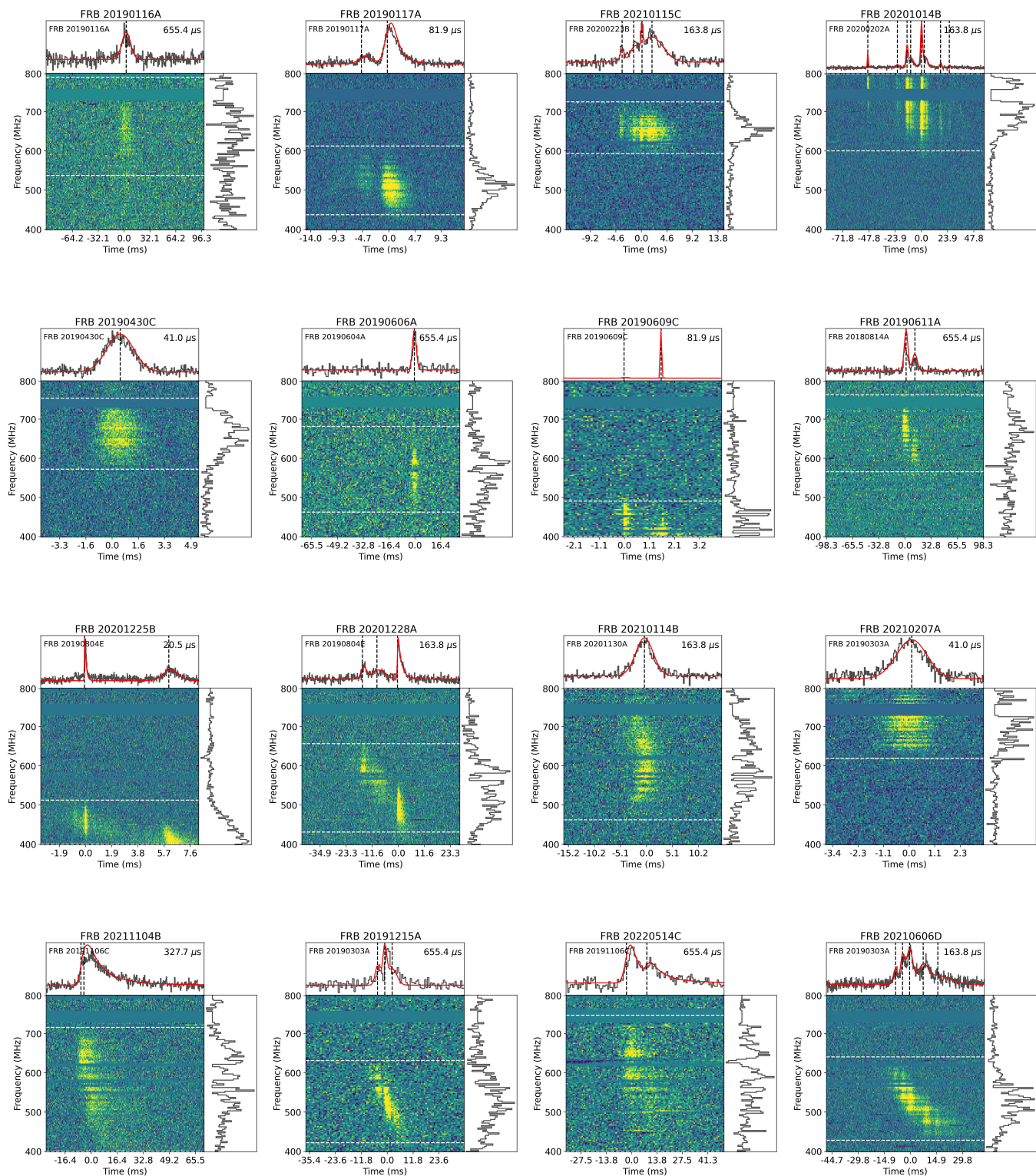


Figure A1. A sub-set of the burst waterfalls from the repeating sources in our sample. Each burst is de-dispersed to its structure maximizing DM, with the relevant `fitburst` fit shown on top of the burst. The time resolution at which the burst is displayed is listed in the top right corner. The dashed, white lines indicated the derived bandwidth range for the source. Channels which were masked due to RFI are shown as dark green/teal. The repeater name is shown in the upper left corner, while the individual burst name is listed on top.

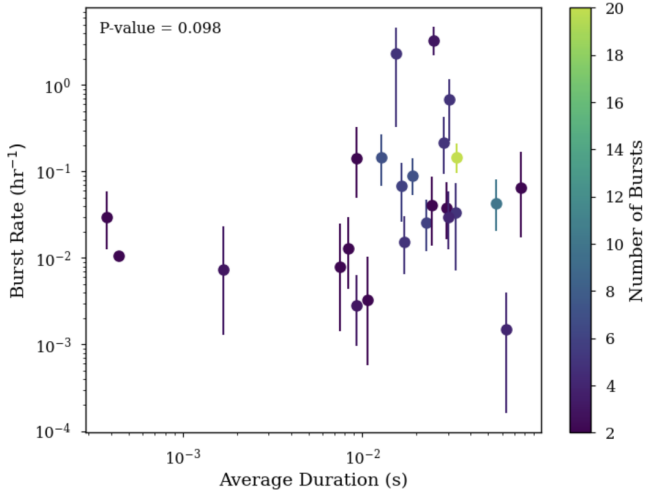


Figure A2. Same as top left panel of Figure 1 except using the maximum burst duration per repeating FRB source.

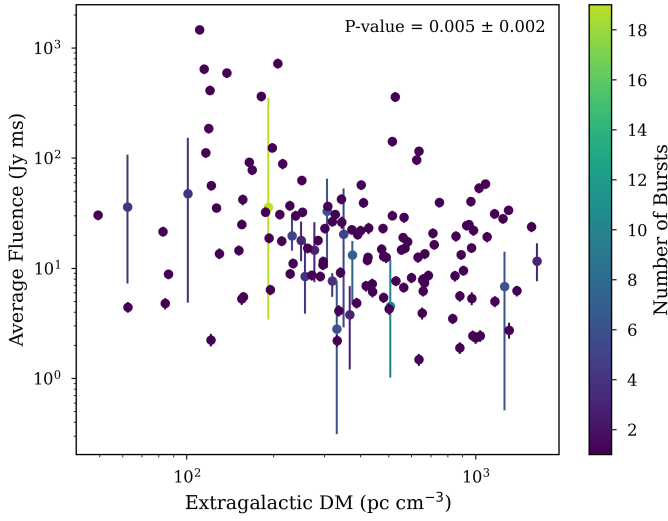


Figure A3. Same as bottom right panel of Figure 1 except including non-repeating FRBs from Sand et al. (2024).

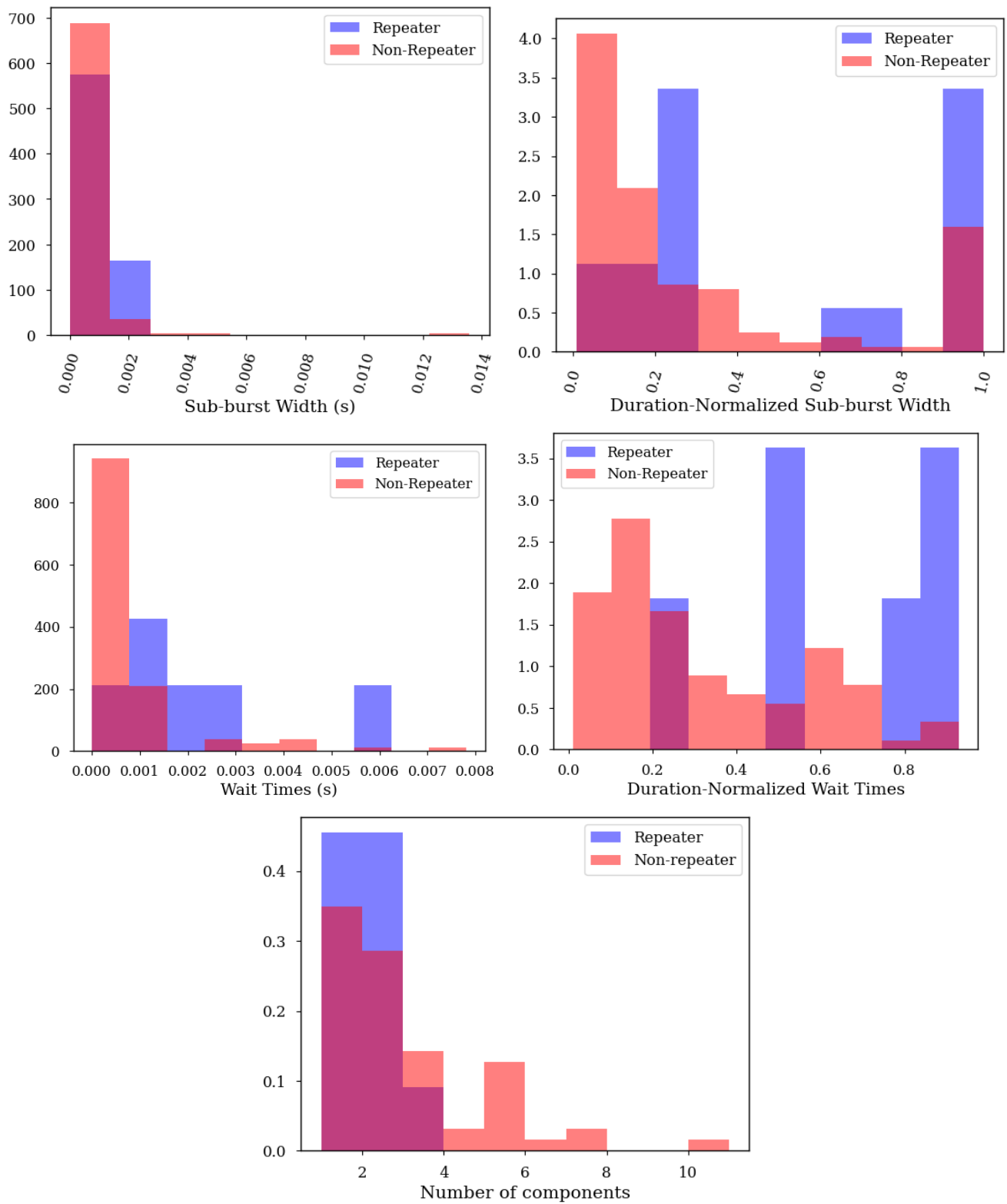


Figure A4. Same as Figure 4 except limiting the burst to those studied at time resolutions $\leq 40 \mu\text{s}$

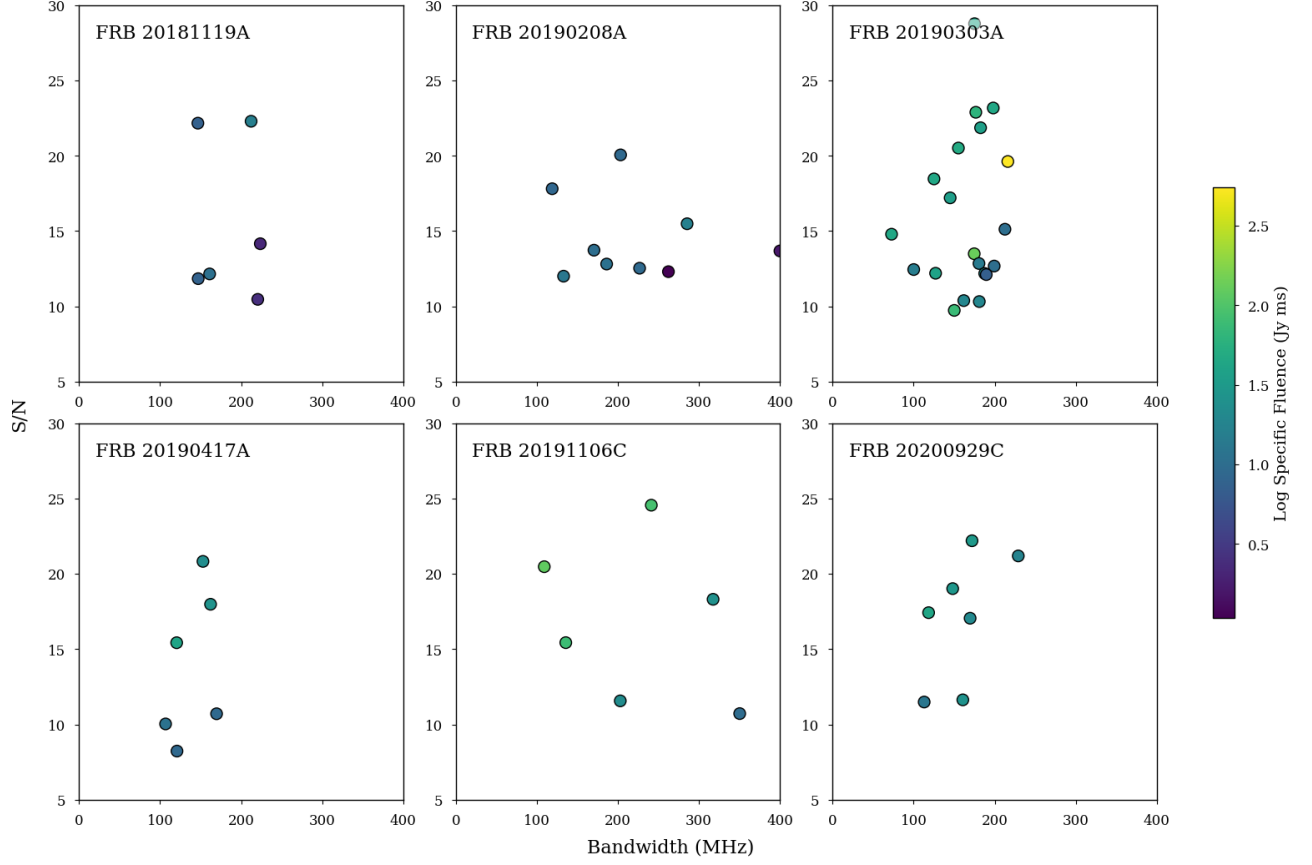


Figure A5. Bandwidth versus detection S/N for all sources in our sample for which there are more than 5 bursts with the complex raw voltages recorded. The color scale indicates the log of the spectral fluence over the spectral extent of the burst.

Table A1. Measured morphological properties for 118 repeating FRBs detected by CHIME/FRB.

TNS Name	Repeater of	t_{res}^a	# Comp. ^b	DM _{struct} ^c	DM _{fit} ^d	Scat. ^e	Duration ^f	BW	Fluence ^g	Flux
		(ms)		(pc cm ⁻³)	(pc cm ⁻³)	(ms)	(ms)	(MHz)	(Jy ms)	(Jy)
FRB 20190611A	FRB 20180814A	0.66	2	189.7(5)	190.20(11)	<2.3	17.3	197.07	22.0(2.3)	2.11(24)
FRB 20190625E	FRB 20180814A	0.66	3	188.53(4)	188.57(4)	<1.1	30.26	78.59	152(16)	15.7(2.2)
FRB 20190626A	FRB 20180814A	0.66	1	191.38(3)	192.24(24)	<8.7	20.38	70.77	–	–
FRB 20191029A	FRB 20180814A	0.66	2	189.129(21)	189.10(10)	<0.66	7.43	157.97	10.2(1.1)	2.01(26)
FRB 20191111C	FRB 20180814A	0.66	2	188.01(–)	188.41(8)	<0.81	6.52	166.96	4.9(6)	0.85(13)
FRB 20190621A	FRB 20180908A	0.66	1	195.81(–)	196.04(15)	<3.1	7.29	59.82	3.9(5)	1.01(24)
FRB 20200621D	FRB 20180910A	0.16	1	696.37(16)	696.297(14)	5.73(22)	2.35	400.0	40(4)	5.9(6)
FRB 20200122A	FRB 20181030A	0.33	2	103.542(12)	103.538(4)	<1.2	62.88	188.86	9.9(1.1)	2.6(3)
FRB 20200122B	FRB 20181030A	0.16	5	103.5(–)	103.501 7(1 4)	<0.11	35.96	234.6	7.3(8)	3.1(3)
FRB 20200122E	FRB 20181030A	0.66	2	103.44(–)	103.55(3)	<0.39	52.35	176.34	107(12)	23(3)
FRB 20200122G	FRB 20181030A	0.16	1	103.53(–)	103.561(15)	<0.71	1.68	246.73	19.0(2.4)	11.6(1.4)
FRB 20200621C	FRB 20181119A	0.66	1	364.11(14)	364.25(11)	<1.2	2.83	147.02	1.95(26)	0.76(13)
FRB 20201204D	FRB 20181119A	0.66	1	364.061(8)	363.93(14)	<1.4	3.37	220.53	1.40(25)	0.88(24)
FRB 20210608B	FRB 20181119A	0.66	1	364.752(16)	364.45(18)	<1.9	4.51	146.63	1.1(3)	0.96(26)
FRB 20210624B	FRB 20181119A	0.66	3	363.61(4)	364.13(20)	<1.2	16.49	212.32	7.7(9)	1.10(20)
FRB 20211111A	FRB 20181119A	0.66	1	364.57(–)	364.86(23)	<2.6	6.11	223.66	0.31(14)	1.02(26)
FRB 20220213A	FRB 20181119A	0.66	1	364.53(–)	364.54(16)	<1.9	4.49	161.09	4.5(6)	2.4(5)
FRB 20201215C	FRB 20181128A	0.66	3	446.976(15)	447.151(28)	<1.5	24.39	228.35	9.2(1.1)	1.60(26)
FRB 20231006C	FRB 20181128A	0.66	2	445.7(4)	446.24(20)	<2.9	19.03	163.05	15.8(1.9)	2.0(4)
FRB 20190110C	FRB 20190110C	0.33	1	222.03(4)	222.051(9)	<0.57	1.35	106.35	5.7(7)	3.5(4)
FRB 20190116A	FRB 20190116A	0.66	1	445.17(10)	445.52(25)	<5.3	12.57	254.15	7.6(8)	1.00(15)
FRB 20190117A	FRB 20190117A	0.08	2	393.018(16)	392.990(5)	0.609(26)	6.71	174.39	24.9(2.5)	6.8(7)
FRB 20211114A	FRB 20190117A	0.16	3	395.89(5)	396.105(20)	<1.7	28.2	173.22	53(5)	4.8(5)
FRB 20230106C	FRB 20190117A	0.66	2	397.21(8)	397.36(7)	0.97(15)	19.6	162.27	8.2(1.2)	2.2(6)
FRB 20230504C	FRB 20190117A	0.66	2	397.1(4)	397.56(13)	<1.6	15.67	240.47	12.8(1.6)	1.6(3)
FRB 20231210C	FRB 20190117A	0.66	1	396.96(–)	397.40(16)	<3.1	7.41	100.88	2.9(4)	1.7(4)
FRB 20200124A	FRB 20190208A	0.66	3	579.88(7)	580.031(25)	<0.79	27.55	285.43	12.0(1.2)	1.56(18)
FRB 20200513B	FRB 20190208A	0.66	2	579.485(9)	579.59(6)	<0.85	33.13	400.0	3.0(4)	1.09(17)
FRB 20210203B	FRB 20190208A	0.08	2	579.824(4)	579.869(7)	1.02(5)	2.06	186.12	4.8(6)	3.5(4)
FRB 20210612B	FRB 20190208A	0.66	2	579.55(5)	580.01(9)	<1.7	13.3	262.37	1.02(22)	1.07(28)
FRB 20211129B	FRB 20190208A	0.33	2	579.823(14)	579.785(16)	<0.78	13.09	170.48	4.2(6)	3.1(4)
FRB 20211205A	FRB 20190208A	0.66	1	579.54(4)	579.83(5)	<1.3	3.07	132.94	4.6(7)	2.1(5)
FRB 20230306D	FRB 20190208A	0.66	2	579.82(17)	579.85(5)	<0.76	6.47	226.78	5.1(7)	2.2(4)
FRB 20211009B	FRB 20190208A	0.66	2	579.92(6)	579.99(4)	<1.1	9.55	118.87	2.7(4)	1.08(24)
FRB 20211228A	FRB 20190208A	0.66	3	579.819(7)	579.759(24)	<0.49	12.34	203.32	4.4(6)	1.41(28)
FRB 20211229A	FRB 20190208A	0.66	6	579.84(4)	579.803(25)	<0.49	55.47	400.0	3.4(5)	1.18(25)
FRB 20191217A	FRB 20190212A	0.66	4	301.6(–)	301.61(5)	<0.99	33.22	287.0	20(2)	2.1(3)
FRB 20200725B	FRB 20190212A	0.66	2	301.56(–)	301.577(7)	<1.3	8.12	120.43	11.6(1.4)	2.5(4)
FRB 20210216B	FRB 20190212A	0.66	2	301.335(16)	301.326(6)	<0.0068	18.23	113.0	15.3(2.2)	9.9(1.8)
FRB 20210410C	FRB 20190212A	0.66	2	301.81(–)	301.795(29)	<0.72	5.37	278.01	7.6(1.2)	4.0(8)
FRB 20210805A	FRB 20190212A	0.66	2	301.37(–)	301.371(8)	<0.47	20.9	175.17	27(5)	17(4)
FRB 20220322C	FRB 20190216A	0.66	1	1279(–)	1 281.83(19)	<19.0	44.12	290.13	1.8(4)	1.2(3)
FRB 20190301A	FRB 20190222A	0.16	2	459.74(–)	459.83(4)	<0.49	4.31	104.01	0.67(12)	0.53(16)
FRB 20190702B	FRB 20190303A	0.04	2	221.26(4)	221.43(3)	2.74(10)	4.08	125.12	20.4(2.1)	2.78(29)
FRB 20191013A	FRB 20190303A	0.66	3	221.43(–)	221.72(6)	<0.94	23.21	150.15	49(5)	3.6(5)
FRB 20191020A	FRB 20190303A	0.16	1	221.61(10)	221.85(5)	1.79(20)	1.29	176.74	13.4(1.7)	5.9(8)
FRB 20191110A	FRB 20190303A	0.16	5	221.43(5)	221.426(10)	<0.85	27.25	155.23	21.3(2.2)	2.05(21)
FRB 20191113A	FRB 20190303A	0.33	5	221.55(7)	221.65(6)	<0.74	28.06	174.78	86(9)	7.0(8)
FRB 20191116A	FRB 20190303A	0.02	3	221.400(27)	221.452(10)	0.95(4)	3.35	175.17	22.0(2.2)	8.8(9)
FRB 20191215A	FRB 20190303A	0.66	3	221.55(4)	221.63(3)	<0.89	10.41	212.71	6.1(6)	0.99(12)

Table A1 *continued*

Table A1 (continued)

TNS Name	Repeater of	t_{res}^a	# Comp. ^b	DM_{struct}^c	DM_{fit}^d	Scat. ^e	Duration ^f	BW	Fluence ^g	Flux
		(ms)		(pc cm ⁻³)	(pc cm ⁻³)	(ms)	(ms)	(MHz)	(Jy ms)	(Jy)
FRB 20191231A	FRB 20190303A	0.66	2	221.42(18)	221.87(9)	<1.2	9.65	181.04	8.6(9)	1.66(22)
FRB 20200112A	FRB 20190303A	0.66	1	221.69(-)	221.53(8)	<3.0	6.97	100.1	4.5(5)	0.63(9)
FRB 20200622A	FRB 20190303A	0.66	1	222.3(4)	222.96(8)	<1.9	4.44	161.88	5.3(6)	1.42(19)
FRB 20210203C	FRB 20190303A	0.08	1	221.73(7)	222.03(6)	<1.3	3.05	127.08	9.0(1.2)	3.7(5)
FRB 20210207A	FRB 20190303A	0.04	1	221.8(4)	221.831(19)	<0.69	1.62	180.65	5.6(7)	3.0(4)
FRB 20210209B	FRB 20190303A	0.01	1	221.66(20)	221.829(8)	<0.73	1.72	182.6	16.3(1.7)	8.4(9)
FRB 20210302C	FRB 20190303A	0.66	3	221.48(4)	221.80(8)	<2.5	27.35	187.68	12.4(1.3)	1.10(15)
FRB 20211014B	FRB 20190303A	0.33	3	221.23(3)	221.43(5)	<0.77	9.23	199.41	5.8(8)	1.60(27)
FRB 20211125A	FRB 20190303A	0.66	2	222(-)	222.42(15)	<1.1	10.88	72.73	19.4(2.3)	4.0(9)
FRB 20210606D	FRB 20190303A	0.16	5	221.26(4)	221.47(3)	<1.1	33.46	216.23	35(4)0	30(3)
FRB 20220214D	FRB 20190303A	0.66	2	221.3(4)	221.86(10)	<2.2	16.19	189.64	3.4(5)	0.94(22)
FRB 20230913E	FRB 20190303A	0.04	1	221.49(7)	221.54(4)	1.84(10)	1.45	145.06	10.7(1.3)	4.5(6)
FRB 20231204A	FRB 20190303A	0.16	3	221.25(4)	221.341(21)	<0.92	9.89	198.24	26.0(2.7)	4.4(5)
FRB 20200726D	FRB 20190417A	0.16	1	1 378.23(26)	1 378.58(6)	3.96(19)	1.91	162.27	7.4(8)	1.90(23)
FRB 20210304B	FRB 20190417A	0.66	1	1 378.81(4)	1 378.59(8)	4.9(3)	2.91	132.55	12.1(1.4)	1.9(3)
FRB 20210404E	FRB 20190417A	0.66	1	1 379.41(10)	1 379.10(19)	3.5(6)	4.3	120.82	2.9(4)	1.2(3)
FRB 20210924B	FRB 20190417A	0.66	1	1 378.60(11)	1 378.6(3)	3.7(5)	3.04	106.74	0.51(22)	2.2(4)
FRB 20220207B	FRB 20190417A	0.66	1	1 378.4(7)	1 378.2(4)	4.4(1.6)	18.99	120.43	14.1(1.6)	1.27(26)
FRB 20220530B	FRB 20190417A	0.66	1	1 379.9(8)	1 379.67(15)	3.8(5)	3.83	169.7	4.3(6)	2.2(5)
FRB 20220619A	FRB 20190417A	0.66	1	1 380.0(5)	1 380.54(11)	4.0(4)	7.63	152.88	11.6(1.4)	1.45(27)
FRB 20190430C	FRB 20190430C	0.04	1	400.36(17)	400.400(15)	<0.83	1.96	181.82	8.8(9)	4.1(4)
FRB 20190606A	FRB 20190604A	0.66	1	552.52(5)	552.60(3)	<1.2	2.8	220.14	3.2(4)	1.22(18)
FRB 20210329A	FRB 20190604A	0.66	1	552.5(5)	552.69(9)	<3.2	7.54	100.88	2.3(3)	0.62(14)
FRB 20190609C	FRB 20190609C	0.08	2	479.86(-)	479.869(4)	<0.0087	1.68	92.28	3.3(4)	4.7(5)
FRB 20201030B	FRB 20190609C	0.02	2	479.796 0(7)	479.793 36(8)	0.01360(22)	1.37	105.18	6.9(8)	35(4)
FRB 20210113D	FRB 20190609C	0.66	1	225.43(10)	479.793(10)	<0.4	0.95	139.59	1.2(3)	2.7(5)
FRB 20200629C	FRB 20190804E	0.66	2	317.75(14)	363.474(29)	<1.5	7.03	180.25	9.0(1.0)	1.96(23)
FRB 20200709C	FRB 20190804E	0.66	2	362.35(-)	362.94(11)	<2.6	13.37	80.94	5.5(6)	0.51(8)
FRB 20201225B	FRB 20190804E	0.02	2	362.724(6)	362.728 4(7)	0.0345(1 1)	6.78	114.17	8.0(1.0)	6.6(7)
FRB 20201228A	FRB 20190804E	0.16	3	362.969(27)	362.963(11)	0.736(26)	17.11	225.22	8.1(1.0)	2.4(3)
FRB 20220203A	FRB 20190804E	0.66	2	362.58(-)	362.90(10)	<1.9	16.55	62.95	-	-
FRB 20200729A	FRB 20190907A	0.33	4	309.12(-)	309.243(20)	<0.81	14.27	393.74	18.0(1.9)	2.30(26)
FRB 20220313B	FRB 20190907A	0.33	2	309.58(13)	309.61(4)	<0.62	3.65	170.48	3.9(5)	2.0(3)
FRB 20220525A	FRB 20190907A	0.66	4	309.31(4)	309.650(19)	<0.34	29.97	156.79	5.6(7)	1.23(21)
FRB 20221207E	FRB 20190907A	0.66	3	309.54(5)	309.76(4)	<1.2	23.49	134.51	6.2(7)	1.53(23)
FRB 20200214B	FRB 20190915D	0.66	1	487.6(3)	489.30(9)	<8.6	20.18	120.43	16.0(1.6)	0.81(10)
FRB 20200515A	FRB 20191013D	0.66	1	522.7(4)	522.43(5)	10.3(7)	5.75	400.0	47(5)	2.8(3)
FRB 20201201A	FRB 20191106C	0.66	1	330.6(-)	333.24(11)	8.2(5)	22.62	109.09	35(4)	1.31(20)
FRB 20210617A	FRB 20191106C	0.66	1	330.6(-)	331.91(7)	9.1(3)	9.34	135.68	44(4)	1.74(22)
FRB 20210822A	FRB 20191106C	0.66	1	331.2(-)	331.09(9)	8.6(7)	3.68	202.93	21.0(2.2)	1.63(24)
FRB 20211104B	FRB 20191106C	0.33	2	331.60(16)	332.10(8)	8.1(3)	6.4	317.5	23.1(2.4)	1.95(28)
FRB 20220118B	FRB 20191106C	0.16	2	330.56(10)	331.031(28)	7.77(13)	10.84	241.25	65(7)	3.4(4)
FRB 20220514C	FRB 20191106C	0.66	2	331.38(11)	331.09(9)	5.9(6)	15.37	350.34	10.1(1.1)	1.00(15)
FRB 20200118D	FRB 20200118D	0.66	2	625.226(21)	625.253(14)	<0.72	7.71	119.26	5.7(6)	1.51(17)
FRB 20200701A	FRB 20200118D	0.08	4	625.290(22)	625.304(7)	<0.32	10.62	377.32	11.5(1.2)	3.7(4)
FRB 20200120E	FRB 20200120E	0.08	1	392.563(4)	87.853(8)	<0.16	0.38	187.68	2.9(3)	3.6(4)
FRB 20210423G	FRB 20200120E	0.01	1	392.83(17)	87.760 70(29)	<0.019	0.04	242.42	1.86(2.4)	14.8(1.5)
FRB 20200127B	FRB 20200127B	0.02	2	351.32(-)	351.346 9(7)	<0.052	0.34	400.0	11.4(1.2)	12.5(1.3)
FRB 20200219B	FRB 20200127B	0.00256	2	275.61(6)	351.274 0(4)	<0.044	0.44	400.0	17.3(1.8)	27.7(2.8)
FRB 20230604B	FRB 20200202A	0.16	1	734.37(26)	734.33(4)	<1.0	2.38	117.3	7.0(9)	3.5(4)
FRB 20201014B	FRB 20200202A	0.16	8	726.5(-)	726.433(9)	<0.38	75.78	199.8	1.36(14)	1.2(3)
FRB 20200702C	FRB 20200223B	0.08	4	200.355(11)	201.01(6)	<0.99	9.24	179.86	40(4)	7.2(7)

Table A1 continued

Table A1 (continued)

TNS Name	Repeater of	t_{res}^a	# Comp. ^b	DM _{struct} ^c	DM _{fit} ^d	Scat. ^e	Duration ^f	BW	Fluence ^g	Flux
		(ms)		(pc cm ⁻³)	(pc cm ⁻³)	(ms)	(ms)	(MHz)	(Jy ms)	(Jy)
FRB 20210115C	FRB 20200223B	0.16	4	200.521(11)	200.57(4)	<0.15	8.12	129.81	17.8(2.1)	5.0(7)
FRB 202101022D	FRB 20200619A	0.66	2	439.86(-)	439.773(11)	<0.17	8.37	400.0	2.1(5)	1.5(3)
FRB 20210130E	FRB 20200619A	0.66	1	413.64(21)	440.25(5)	<2.1	4.91	114.57	-	-
FRB 20200809E	FRB 20200809E	0.66	1	1 702.89(10)	1 703.04(4)	<2.0	4.6	72.34	10.4(1.1)	2.5(3)
FRB 20201018C	FRB 20200809E	0.33	2	1 702.86(3)	1 703.08(3)	<0.43	4.86	260.41	16.8(1.8)	4.1(5)
FRB 20210208B	FRB 20200809E	0.66	2	1 703.358(22)	1 703.67(17)	<0.75	9.32	169.7	7.6(1.0)	2.0(4)
FRB 20230725D	FRB 20200926A	0.16	3	758.63(3)	758.475(21)	<0.74	11.85	162.27	16.0(1.8)	3.4(4)
FRB 20201125B	FRB 20200929C	0.08	1	413.67(7)	413.740(9)	<0.88	2.08	229.13	11.9(1.3)	5.7(6)
FRB 20201203C	FRB 20200929C	0.66	1	413.54(4)	413.57(3)	<1.2	2.78	113.0	4.7(6)	2.0(4)
FRB 20210313B	FRB 20200929C	0.16	1	413.67(11)	413.599(8)	<1.8	4.27	118.48	17.0(1.9)	4.9(6)
FRB 20210314A	FRB 20200929C	0.66	2	413.54(17)	413.600(25)	<1.2	7.76	169.7	11.2(1.6)	3.8(7)
FRB 20210326B	FRB 20200929C	0.08	1	413.75(12)	413.749(4)	<1.6	3.83	172.04	17.7(2.0)	4.9(6)
FRB 20210930A	FRB 20200929C	0.66	2	413.43(19)	413.775(7)	<2.0	12.67	160.7	15.5(1.8)	2.5(4)
FRB 20220209A	FRB 20200929C	0.16	2	413.20(7)	413.354(11)	<1.1	7.04	148.19	14.6(1.8)	4.4(7)
FRB 20201219A	FRB 20201114A	0.66	2	321.31(13)	321.47(10)	<2.2	10.57	144.28	8.0(9)	1.55(22)
FRB 20210327A	FRB 20201124A	0.66	2	415.49(-)	415.6(4)	<5.3	24.88	219.35	10.4(1.1)	1.38(25)
FRB 20210331A	FRB 20201124A	0.66	1	416.2(-)	416.50(24)	<6.2	14.54	232.65	7.4(9)	0.92(18)
FRB 20201225D	FRB 20201130A	0.66	1	287.6(5)	288.32(7)	<4.8	11.21	274.88	18.2(2.0)	2.6(4)
FRB 20210114B	FRB 20201130A	0.16	1	288.27(25)	288.381(21)	<1.7	4.03	337.44	16.8(1.9)	4.5(6)
FRB 20210117E	FRB 20201130A	0.66	2	287.83(10)	287.96(7)	<2.8	15.32	135.68	14.3(1.6)	2.4(4)
FRB 20210118B	FRB 20201130A	0.16	1	288.0(5)	288.39(3)	<2.7	6.39	310.07	20.1(2.3)	4.1(6)
FRB 20210327F	FRB 20201130A	0.33	1	287.68(11)	287.66(4)	<4.1	9.61	257.28	29(3)	4.2(5)
FRB 20210302E	FRB 20201221B	0.66	3	430.43(3)	510.59(6)	<1.6	29.32	160.7	-	-
FRB 20210303F	FRB 20201221B	0.66	2	509.72(15)	510.35(8)	<4.6	27.27	89.54	16.5(1.7)	1.19(16)

^a Time resolution at which the burst is analyzed and parameters are reported.

^b Number of visible sub-bursts at the given time resolution for the burst.

^c Structure maximizing DM.

^d DM determined using the `fitburst` routine.

^e Scattering time as determined using `fitburst`. If no visible scattering by-eye, an upper limit on the scattering timescale is set to be equal to the reported `fitburst` width of the narrowest sub-component. Scattering timescales are referenced to 600 MHz.

^f Total duration of the burst.

^g Spectral fluence over the entire 400 to 800 MHz CHIME/FRB band.

REFERENCES

- 2008, Kolmogorov–Smirnov Test (New York, NY: Springer New York), 283–287, doi: [10.1007/978-0-387-32833-1_214](https://doi.org/10.1007/978-0-387-32833-1_214)
- Andersen, B. C., Patel, C., Brar, C., et al. 2023, *AJ*, 166, 138, doi: [10.3847/1538-3881/acec78](https://doi.org/10.3847/1538-3881/acec78)
- Anderson, T. W., & Darling, D. A. 1954, *Journal of the American Statistical Association*, 49, 765, doi: [10.1080/01621459.1954.10501232](https://doi.org/10.1080/01621459.1954.10501232)
- Anna-Thomas, R., Connor, L., Dai, S., et al. 2023, *Science*, 380, 599–603, doi: [10.1126/science.abo6526](https://doi.org/10.1126/science.abo6526)
- Bethapudi, S., Spitler, L. G., Main, R. A., Li, D. Z., & Wharton, R. S. 2022, arXiv e-prints, arXiv:2207.13669. <https://arxiv.org/abs/2207.13669>
- Bhardwaj, M., Gaensler, B. M., Kaspi, V. M., et al. 2021, *The Astrophysical Journal Letters*, 910, L18, doi: [10.3847/2041-8213/abeaa6](https://doi.org/10.3847/2041-8213/abeaa6)
- Bhardwaj, M., Gaensler, B. M., Kaspi, V. M., et al. 2021, *ApJL*, 910, L18, doi: [10.3847/2041-8213/abeaa6](https://doi.org/10.3847/2041-8213/abeaa6)

Table A2. Burst Rates

Source	N_{bursts}^a	Exposure ^b (hr ⁻¹)	Threshold ^c (Jy ms)	Burst Rate ^e (hr ⁻¹)
FRB 20201130A	5	43.9	16.1	$0.020^{+0.026}_{-0.013}$
FRB 20191106C	0	2.0	30.6	$0.0^{+0.12}$
FRB 20200619A	4	209.0	2.3	$0.061^{+0.095}_{-0.044}$
FRB 20190804E	4	176.6	4.4	$0.027^{+0.042}_{-0.020}$
FRB 20190915D	4	178.5	10.7	$0.007^{+0.011}_{-0.0052}$
FRB 20200929C	0	0.0	4.6	—
FRB 20201221B	1	1.5	16.1	$0.11^{+0.52}_{-0.11}$
FRB 20200809E	3	914.0	10.0	$0.0012^{+0.0022}_{-0.00092}$
FRB 20190609C	2	133.7	4.4	$0.018^{+0.047}_{-0.016}$
FRB 20200223B	4	1.6	22.3	$0.27^{+0.42}_{-0.20}$
FRB 20200202A	2	110.7	2.1	$0.07^{+0.18}_{-0.059}$
FRB 20190430C	3	57.7	6.4	$0.036^{+0.069}_{-0.029}$
FRB 20200127B	0	252.5	6.7	$0.0^{+0.009}$
FRB 20201114A	0	237.9	13.4	$0.0^{+0.004}$
FRB 20190110C	0	88.6	1.7	$0.0^{+0.2}$
FRB 20200118D	1	139.1	3.8	$0.011^{+0.049}_{-0.010}$
FRB 20191013D	1	126.4	12.4	$0.0020^{+0.0092}_{-0.0020}$
FRB 20200926A	5	205.4	8.9	$0.010^{+0.014}_{-0.0069}$
FRB 20180910A	0	7400.7	10.7	$0.0^{+0.0002}$
FRB 20180814A	8	426.6	5.1	$0.018^{+0.018}_{-0.010}$
FRB 20181030A	2	396.0	6.7	$0.0033^{+0.0085}_{-0.0029}$
FRB 20181128A	9	184.2	6.7	$0.032^{+0.028}_{-0.017}$
FRB 20181119A	13	266.8	1.6	$0.26^{+0.19}_{-0.12}$
FRB 20190116A	2	127.7	9.4	$0.006^{+0.016}_{-0.0053}$
FRB 20190216A	4	322.0	6.7	$0.008^{+0.013}_{-0.0059}$
FRB 20190222A	0	307.1	0.2	$0.0^{+1.55}$
FRB 20190208A	15	173.8	4.5	$0.102^{+0.066}_{-0.045}$
FRB 20190604A	3	191.1	4.6	$0.018^{+0.034}_{-0.014}$
FRB 20190212A	0	60.8	3.4	$0.0^{+0.11}$
FRB 20180908A	—	—	—	—
FRB 20190117A	15	127.7	20.1	$0.0145^{+0.0094}_{-0.0064}$
FRB 20190303A	1	78.5	4.1	$0.017^{+0.079}_{-0.017}$
FRB 20190417A	12	213.5	1.6	$0.32^{+0.24}_{-0.15}$
FRB 20190907A	5	127.5	7.0	$0.024^{+0.032}_{-0.016}$
FRB 20200120E	7	315.6	3.8	$0.033^{+0.035}_{-0.020}$
FRB 20201124A	23	92.8	26.1	$0.021^{+0.010}_{-0.0076}$

^a Number of bursts detected from this source that fall within the FWHM at 600 MHz of the corresponding detection beam. If a source has both a lower and upper transit, only bursts within the upper transit are considered.

^b Total exposure to the position of this source. For sources observed twice a day, this corresponds to the exposure solely in the upper transit.

^c Fluence threshold for the source at the 95% confidence level (only upper transit).

^d Burst rate (in upper transit; if applicable) scaled to a fluence threshold of 5 Jy ms.

Bhat, N. D. R., Cordes, J. M., Camilo, F., Nice, D. J., & Lorimer, D. R. 2004, *The Astrophysical Journal*, 605, 759–783, doi: [10.1086/382680](https://doi.org/10.1086/382680)

Bochenek, C. D., Ravi, V., Belov, K. V., et al. 2020, *Nature*, 587, 59

Caleb, M., Driessen, L. N., Gordon, A. C., et al. 2023, *MNRAS*, 524, 2064, doi: [10.1093/mnras/stad1839](https://doi.org/10.1093/mnras/stad1839)

Chawla, P., Kaspi, V. M., Ransom, S. M., et al. 2022, *ApJ*, 927, 35, doi: [10.3847/1538-4357/ac49e1](https://doi.org/10.3847/1538-4357/ac49e1)

Chikada, Y., Ishiguro, M., Hirabayashi, H., et al. 1984, in *Indirect Imaging. Measurement and Processing for Indirect Imaging*, ed. J. A. Roberts, 387

CHIME Collaboration, Amiri, M., Bandura, K., Boskovic, A., et al. 2022, *The Astrophysical Journal Supplement Series*, 261, 29, doi: [10.3847/1538-4365/ac6fd9](https://doi.org/10.3847/1538-4365/ac6fd9)

CHIME/FRB Collaboration, Amiri, M., Bandura, K., et al. 2018, *ApJ*, 863, 48, doi: [10.3847/1538-4357/aad188](https://doi.org/10.3847/1538-4357/aad188)

—. 2019a, *Nature*, 566, 235, doi: [10.1038/s41586-018-0864-x](https://doi.org/10.1038/s41586-018-0864-x)

CHIME/FRB Collaboration, Andersen, B. C., Bandura, K., et al. 2019b, *ApJL*, 885, L24, doi: [10.3847/2041-8213/ab4a80](https://doi.org/10.3847/2041-8213/ab4a80)

CHIME/FRB Collaboration, Amiri, M., Andersen, B. C., et al. 2020a, *Nature*, 582, 351, doi: [10.1038/s41586-020-2398-2](https://doi.org/10.1038/s41586-020-2398-2)

CHIME/FRB Collaboration, Andersen, B., Bandura, K., et al. 2020b, *Nature*, 587, 54

CHIME/FRB Collaboration, Amiri, M., Andersen, B. C., et al. 2021, *ApJS*, 257, 59, doi: [10.3847/1538-4365/ac33ab](https://doi.org/10.3847/1538-4365/ac33ab)

CHIME/FRB Collaboration, Andersen, B. C., Bandura, K., et al. 2023a, *ApJ*, 947, 83, doi: [10.3847/1538-4357/acc6c1](https://doi.org/10.3847/1538-4357/acc6c1)

CHIME/FRB Collaboration, :, Amiri, M., et al. 2023b, *arXiv e-prints*, arXiv:2311.00111, doi: [10.48550/arXiv.2311.00111](https://doi.org/10.48550/arXiv.2311.00111)

CHIME/FRB Collaboration, Amiri, M., Andersen, B. C., et al. 2024, *ApJ*, 969, 145, doi: [10.3847/1538-4357/ad464b](https://doi.org/10.3847/1538-4357/ad464b)

CHIME/FRB Collaboration, Andersen, B. C., Bandura, K., Bhardwaj, M., et al. 2022, *Nature*, 607, 256, doi: [10.1038/s41586-022-04841-8](https://doi.org/10.1038/s41586-022-04841-8)

Cho, H., Macquart, J.-P., Shannon, R. M., et al. 2020, *ApJL*, 891, L38, doi: [10.3847/2041-8213/ab7824](https://doi.org/10.3847/2041-8213/ab7824)

Connor, L. 2019, *MNRAS*, 487, 5753, doi: [10.1093/mnras/stz1666](https://doi.org/10.1093/mnras/stz1666)

Connor, L., Miller, M. C., & Gardenier, D. W. 2020, *MNRAS*, 497, 3076, doi: [10.1093/mnras/staa2074](https://doi.org/10.1093/mnras/staa2074)

Cook, A. M., Bhardwaj, M., Gaensler, B. M., et al. 2023, *ApJ*, 946, 58, doi: [10.3847/1538-4357/acbbd0](https://doi.org/10.3847/1538-4357/acbbd0)

Cordes, J. M., & Lazio, T. J. W. 2002, *arXiv e-prints*, astro, doi: [10.48550/arXiv.astro-ph/0207156](https://doi.org/10.48550/arXiv.astro-ph/0207156)

Cordes, J. M., & Lazio, T. J. W. 2002, *arXiv preprint astro-ph/0207156*

Das, S., Mathur, S., Gupta, A., Nicastro, F., & Krongold, Y. 2021, *MNRAS*, 500, 655, doi: [10.1093/mnras/staa3299](https://doi.org/10.1093/mnras/staa3299)

- Desvignes, G., Eatough, R. P., Pen, U. L., et al. 2018, *ApJL*, 852, L12, doi: [10.3847/2041-8213/aaa2f8](https://doi.org/10.3847/2041-8213/aaa2f8)
- Faber, J. T., Michilli, D., Mckinven, R., et al. 2023, arXiv e-prints, arXiv:2312.14133, doi: [10.48550/arXiv.2312.14133](https://doi.org/10.48550/arXiv.2312.14133)
- Farah, W., Flynn, C., Bailes, M., et al. 2018, *MNRAS*, 478, 1209, doi: [10.1093/mnras/sty1122](https://doi.org/10.1093/mnras/sty1122)
- Fonseca, E., Andersen, B. C., Bhardwaj, M., et al. 2020, *ApJL*, 891, L6, doi: [10.3847/2041-8213/ab7208](https://doi.org/10.3847/2041-8213/ab7208)
- Fonseca, E., Pleunis, Z., Breitman, D., et al. 2023, arXiv e-prints, arXiv:2311.05829, doi: [10.48550/arXiv.2311.05829](https://doi.org/10.48550/arXiv.2311.05829)
- Foreman-Mackey, D., Hogg, D. W., Lang, D., & Goodman, J. 2013, *PASP*, 125, 306, doi: [10.1086/670067](https://doi.org/10.1086/670067)
- Gajjar, V., Siemion, A. P. V., Price, D. C., et al. 2018, *ApJ*, 863, 2, doi: [10.3847/1538-4357/aad005](https://doi.org/10.3847/1538-4357/aad005)
- Hessels, J. W. T., Spitler, L. G., Seymour, A. D., et al. 2019, *The Astrophysical Journal Letters*, 876, L23, doi: [10.3847/2041-8213/ab13ae](https://doi.org/10.3847/2041-8213/ab13ae)
- Hessels, J. W. T., Spitler, L. G., Seymour, A. D., et al. 2019, *ApJL*, 876, L23, doi: [10.3847/2041-8213/ab13ae](https://doi.org/10.3847/2041-8213/ab13ae)
- Hewitt, D. M., Hessels, J. W. T., Ould-Boukattine, O. S., et al. 2023, *MNRAS*, 526, 2039, doi: [10.1093/mnras/stad2847](https://doi.org/10.1093/mnras/stad2847)
- Ioka, K. 2020, *ApJL*, 904, L15, doi: [10.3847/2041-8213/abc6a3](https://doi.org/10.3847/2041-8213/abc6a3)
- James, C. W. 2023, *PASA*, 40, e057, doi: [10.1017/pasa.2023.51](https://doi.org/10.1017/pasa.2023.51)
- Josephy, A., Chawla, P., Fonseca, E., et al. 2019, *ApJL*, 882, L18, doi: [10.3847/2041-8213/ab2c00](https://doi.org/10.3847/2041-8213/ab2c00)
- Khrykin, I. S., Ata, M., Lee, K.-G., et al. 2024, arXiv e-prints, arXiv:2402.00505, doi: [10.48550/arXiv.2402.00505](https://doi.org/10.48550/arXiv.2402.00505)
- Kirsten, F., Snelders, M. P., Jenkins, M., et al. 2021, *Nature Astronomy*, 5, 414, doi: [10.1038/s41550-020-01246-3](https://doi.org/10.1038/s41550-020-01246-3)
- Kirsten, F., Marcote, B., Nimmo, K., et al. 2022, *Nature*, 602, 585, doi: [10.1038/s41586-021-04354-w](https://doi.org/10.1038/s41586-021-04354-w)
- Kirsten, F., Ould-Boukattine, O. S., Herrmann, W., et al. 2024, *Nature Astronomy*, 8, 337, doi: [10.1038/s41550-023-02153-z](https://doi.org/10.1038/s41550-023-02153-z)
- Konijn, D. C., Hewitt, D. M., Hessels, J. W. T., et al. 2024, arXiv e-prints, arXiv:2407.10155, doi: [10.48550/arXiv.2407.10155](https://doi.org/10.48550/arXiv.2407.10155)
- Kramer, M., Liu, K., Desvignes, G., Karuppusamy, R., & Stappers, B. W. 2024, *Nature Astronomy*, 8, 230, doi: [10.1038/s41550-023-02125-3](https://doi.org/10.1038/s41550-023-02125-3)
- Lanman, A. E., Andersen, B. C., Chawla, P., et al. 2022, *ApJ*, 927, 59, doi: [10.3847/1538-4357/ac4bc7](https://doi.org/10.3847/1538-4357/ac4bc7)
- Lanman, A. E., Andrew, S., Lazda, M., et al. 2024, arXiv e-prints, arXiv:2402.07898, doi: [10.48550/arXiv.2402.07898](https://doi.org/10.48550/arXiv.2402.07898)
- Lopaka, L. 2020, *NADA: Nondetects and Data Analysis for Environmental Data*. <https://CRAN.R-project.org/package=NADA>
- Lorimer, D. R., Bailes, M., McLaughlin, M. A., Narkevic, D. J., & Crawford, F. 2007, *Science*, 318, 777. <https://arxiv.org/abs/0709.4301>
- Lu, W., & Kumar, P. 2018, *Monthly Notices of the Royal Astronomical Society*, 477, 2470
- Macquart, J.-P., & Koay, J. Y. 2013, *ApJ*, 776, 125, doi: [10.1088/0004-637X/776/2/125](https://doi.org/10.1088/0004-637X/776/2/125)
- Majid, W. A., Pearلمان, A. B., Prince, T. A., et al. 2021, *ApJL*, 919, L6, doi: [10.3847/2041-8213/ac1921](https://doi.org/10.3847/2041-8213/ac1921)
- Marcote, B., Paragi, Z., Hessels, J. W. T., et al. 2017, *The Astrophysical Journal Letters*, 834, L8, doi: [10.3847/2041-8213/834/2/18](https://doi.org/10.3847/2041-8213/834/2/18)
- Margalit, B., Metzger, B. D., & Sironi, L. 2020, *MNRAS*, 494, 4627, doi: [10.1093/mnras/staa1036](https://doi.org/10.1093/mnras/staa1036)
- McKinnon, M. M. 2014, *PASP*, 126, 476, doi: [10.1086/676975](https://doi.org/10.1086/676975)
- Mckinven, R., Gaensler, B. M., Michilli, D., et al. 2023a, *ApJ*, 951, 82, doi: [10.3847/1538-4357/acd188](https://doi.org/10.3847/1538-4357/acd188)
- . 2023b, *ApJ*, 951, 82, doi: [10.3847/1538-4357/acd188](https://doi.org/10.3847/1538-4357/acd188)
- Mckinven, R., Bhardwaj, M., Eftekhari, T., et al. 2024, A pulsar-like swing in the polarisation position angle of a nearby fast radio burst. <https://arxiv.org/abs/2402.09304>
- Merryfield, M., Tendulkar, S. P., Shin, K., et al. 2023, *AJ*, 165, 152, doi: [10.3847/1538-3881/ac9ab5](https://doi.org/10.3847/1538-3881/ac9ab5)
- Metzger, B. D., Margalit, B., & Sironi, L. 2019, *MNRAS*, 485, 4091, doi: [10.1093/mnras/stz700](https://doi.org/10.1093/mnras/stz700)
- Michilli, D., Seymour, A., Hessels, J., et al. 2018, *Nature*, 553, 182
- Michilli, D., Masui, K. W., Mckinven, R., et al. 2021, *ApJ*, 910, 147, doi: [10.3847/1538-4357/abe626](https://doi.org/10.3847/1538-4357/abe626)
- Michilli, D., Bhardwaj, M., Brar, C., et al. 2023, *The Astrophysical Journal*, 950, 134, doi: [10.3847/1538-4357/accf89](https://doi.org/10.3847/1538-4357/accf89)
- Ng, C., Vanderlinde, K., Paradise, A., et al. 2017, in *Proceedings of XXXIInd General Assembly and Scientific Symposium of the International Union of Radio Science (URSI GASS)*, 1–4, doi: [10.23919/URSIGASS.2017.8105318](https://doi.org/10.23919/URSIGASS.2017.8105318)
- Nimmo, K., Hessels, J. W. T., Keimpema, A., et al. 2021, *Nature Astronomy*, 5, 594, doi: [10.1038/s41550-021-01321-3](https://doi.org/10.1038/s41550-021-01321-3)
- Nimmo, K., Hessels, J., Kirsten, F., et al. 2022, *Nature Astronomy*, 1

- Nimmo, K., Pleunis, Z., Beniamini, P., et al. 2024, arXiv e-prints, arXiv:2406.11053, doi: [10.48550/arXiv.2406.11053](https://doi.org/10.48550/arXiv.2406.11053)
- Ocker, S. K., Cordes, J. M., Chatterjee, S., & Gorsuch, M. R. 2022a, *ApJ*, 934, 71, doi: [10.3847/1538-4357/ac75ba](https://doi.org/10.3847/1538-4357/ac75ba)
- Ocker, S. K., Cordes, J. M., Chatterjee, S., et al. 2022b, *ApJ*, 931, 87, doi: [10.3847/1538-4357/ac6504](https://doi.org/10.3847/1538-4357/ac6504)
- Ould-Boukattine, O. S., Chawla, P., Hessels, J. W. T., et al. 2024, A probe of the maximum energetics of fast radio bursts through a prolific repeating source. <https://arxiv.org/abs/2410.17024>
- Pandhi, A., Pleunis, Z., Mckinven, R., et al. 2024, *ApJ*, 968, 50, doi: [10.3847/1538-4357/ad40aa](https://doi.org/10.3847/1538-4357/ad40aa)
- Pandhi, A., Pleunis, Z., Mckinven, R., et al. 2024, Polarization properties of 128 non-repeating fast radio bursts from the first CHIME/FRB baseband catalog. <https://arxiv.org/abs/2401.17378>
- Pastor-Marazuela, I., Connor, L., van Leeuwen, J., et al. 2021, *Nature*, 596, 505, doi: [10.1038/s41586-021-03724-8](https://doi.org/10.1038/s41586-021-03724-8)
- Peto, R., & Peto, J. 1972, *Journal of the Royal Statistical Society. Series A (General)*, 135, 185. <http://www.jstor.org/stable/2344317>
- Petroff, E., Keith, M. J., Johnston, S., van Straten, W., & Shannon, R. M. 2013, *MNRAS*, 435, 1610, doi: [10.1093/mnras/stt1401](https://doi.org/10.1093/mnras/stt1401)
- Piro, A. L., & Gaensler, B. M. 2018, *ApJ*, 861, 150, doi: [10.3847/1538-4357/aac9bc](https://doi.org/10.3847/1538-4357/aac9bc)
- Pleunis, Z., Good, D. C., Kaspi, V. M., et al. 2021a, *ApJ*, 923, 1, doi: [10.3847/1538-4357/ac33ac](https://doi.org/10.3847/1538-4357/ac33ac)
- Pleunis, Z., Michilli, D., Bassa, C. G., et al. 2021b, *ApJL*, 911, L3, doi: [10.3847/2041-8213/abec72](https://doi.org/10.3847/2041-8213/abec72)
- R Core Team. 2020, *R: A Language and Environment for Statistical Computing*, R Foundation for Statistical Computing, Vienna, Austria. <https://www.R-project.org/>
- Rafiei-Ravandi, M., & Smith, K. M. 2022, arXiv e-prints, arXiv:2206.07292. <https://arxiv.org/abs/2206.07292>
- Sand, K. R., Breitman, D., Michilli, D., et al. 2023, *ApJ*, 956, 23, doi: [10.3847/1538-4357/acf221](https://doi.org/10.3847/1538-4357/acf221)
- Sand, K. R., Curtin, A. P., Michilli, D., et al. 2024, arXiv e-prints, arXiv:2408.13215, doi: [10.48550/arXiv.2408.13215](https://doi.org/10.48550/arXiv.2408.13215)
- Seabold, S., & Perktold, J. 2010, in 9th Python in Science Conference
- Seymour, A., Michilli, D., & Pleunis, Z. 2019, DM-phase: Algorithm for correcting dispersion of radio signals. <http://ascl.net/1910.004>
- Sheikh, S. Z., Farah, W., Pollak, A. W., et al. 2024, *MNRAS*, 527, 10425, doi: [10.1093/mnras/stad3630](https://doi.org/10.1093/mnras/stad3630)
- Shin, K., Masui, K. W., Bhardwaj, M., et al. 2023, *ApJ*, 944, 105, doi: [10.3847/1538-4357/acaf06](https://doi.org/10.3847/1538-4357/acaf06)
- Spearman, C. 1904, *The American Journal of Psychology*, 15, 201, doi: [10.2307/1412107](https://doi.org/10.2307/1412107)
- Spitler, L. G., Scholz, P., Hessels, J. W. T., et al. 2016, *Nature*, 531, 202, doi: [10.1038/nature17168](https://doi.org/10.1038/nature17168)
- Virtanen, P., Gommers, R., Oliphant, T. E., et al. 2020, *Nature Methods*, 17, 261–272, doi: [10.1038/s41592-019-0686-2](https://doi.org/10.1038/s41592-019-0686-2)
- Virtanen, P., Gommers, R., Oliphant, T. E., et al. 2020, *Nature Methods*, 17, 261, doi: [10.1038/s41592-019-0686-2](https://doi.org/10.1038/s41592-019-0686-2)
- Wang, W., Zhang, B., Chen, X., & Xu, R. 2019, *ApJL*, 876, L15, doi: [10.3847/2041-8213/ab1aab](https://doi.org/10.3847/2041-8213/ab1aab)
- Xu, H., Niu, J. R., Chen, P., et al. 2022, *Nature*, 609, 685, doi: [10.1038/s41586-022-05071-8](https://doi.org/10.1038/s41586-022-05071-8)
- Yamasaki, S., & Totani, T. 2020, *ApJ*, 888, 105, doi: [10.3847/1538-4357/ab58c4](https://doi.org/10.3847/1538-4357/ab58c4)
- Yang, Y.-P., & Zhang, B. 2016, *ApJL*, 830, L31. <https://arxiv.org/abs/1608.08154>